HHS Public Access

Author manuscript

Cell Rep. Author manuscript; available in PMC 2024 February 08.

Published in final edited form as:

Cell Rep. 2024 January 23; 43(1): 113626. doi:10.1016/j.celrep.2023.113626.

CHCHD4-TRIAP1 regulation of innate immune signaling mediates skeletal muscle adaptation to exercise

Jin Ma[1,4], **Ping-yuan Wang**[1,4], **Jie Zhuang**[1,2], **Annie Y. Son**[1], **Alexander K. Karius**[1], **Abu Mohammad Syed**[1], **Masahiro Nishi**[1], **Zhichao Wu**[3], **Mateus P. Mori**[1], **Young-Chae Kim**[1], **Paul M. Hwang**[1,5,*]

[1]Cardiovascular Branch, National Heart, Lung, and Blood Institute (NHLBI), NIH, Bethesda, MD 20892, USA

[2]School of Medicine, Nankai University, Tianjin 300071, China

[3]Laboratory of Pathology, National Cancer Institute (NCI), NIH, Bethesda, MD 20892, USA

[4]These authors contributed equally

[5]Lead contact

SUMMARY

Exercise training can stimulate the formation of fatty-acid-oxidizing slow-twitch skeletal muscle fibers, which are inversely correlated with obesity, but the molecular mechanism underlying this transformation requires further elucidation. Here, we report that the downregulation of the mitochondrial disulfide relay carrier CHCHD4 by exercise training decreases the import of TP53-regulated inhibitor of apoptosis 1 (TRIAP1) into mitochondria, which can reduce cardiolipin levels and promote VDAC oligomerization in skeletal muscle. VDAC oligomerization, known to facilitate mtDNA release, can activate cGAS-STING/NFKB innate immune signaling and downregulate MyoD in skeletal muscle, thereby promoting the formation of oxidative slow-twitch fibers. In mice, CHCHD4 haploinsufficiency is sufficient to activate this pathway, leading to increased oxidative muscle fibers and decreased fat accumulation with aging. The identification of a specific mediator regulating muscle fiber transformation provides an opportunity to understand further the molecular underpinnings of complex metabolic conditions such as obesity and could have therapeutic implications.

Graphical Abstract

*Correspondence: hwangp@mail.nih.gov.

AUTHOR CONTRIBUTIONS

P.W., J.M., and P.M.H. conceived the project. P.M.H. secured the funding. P.W., J.M., J.Z., A.Y.S., and P.M.H. designed the experiments. P.W., J.M., J.Z., A.Y.S., A.K.K., A.M.S., M.N., and Y.-C.K. carried out the experiments. P.W., J.M., J.Z., A.Y.S., A.K.K., A.M.S., M.N., Z.W., M.P.M., Y.-C.K., and P.M.H. analyzed the data. P.W., J.M., and P.M.H. wrote the manuscript. A.Y.S. and Y.-C.K. edited the manuscript. P.W. and J.M. worked together equally over the course of the project and agreed to cofirst authorships in the listed order.

DECLARATION OF INTERESTS

The authors declare no competing interests.

SUPPLEMENTAL INFORMATION

Supplemental information can be found online at https://doi.org/10.1016/j.celrep.2023.113626.

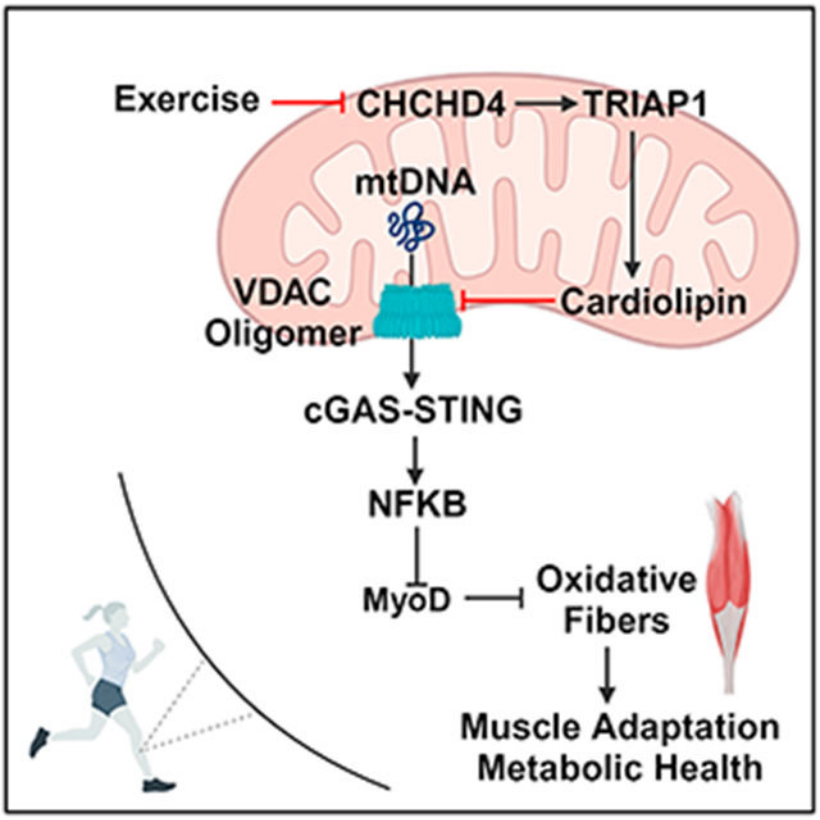

In brief

Oxidative slow-twitch muscle fibers are inversely correlated with obesity. Ma et al. show that exercise-induced downregulation of CHCHD4, a mitochondrial protein import carrier, activates NFKB via innate immune signaling pathway, which in turn inhibits MyoD with resultant increases in oxidative fiber type. Modulating this signaling pathway may prevent obesity.

INTRODUCTION

Skeletal muscle makes up approximately 40% of human body mass and plays an important role in the homeostasis of glucose and fatty acids, which are dysregulated in insulin-resistance and obesity disorders.[1] It is a dynamic tissue composed of different contractile fiber types that can undergo changes with neural activity and exercise training, resulting in increased slow-twitch (type I) fibers with a propensity for oxidative metabolism.[2] Because they are enriched in mitochondria and myoglobin, type I fibers have an increased capacity for cellular energy generation via fatty acid oxidation and are relatively fatigue resistant, contributing to the phenotype of increased exercise endurance.[3] In humans, slow-twitch fibers have been inversely associated with body fat composition and cardiac risk factors and, thus, thought to be protective against the various diseases associated with obesity.[4-6] In contrast to the effects of exercise training, increased caloric intake with a sedentary lifestyle, associated with obesity and insulin resistance, may result in slow- to fast-twitch fiber type switching.[1]

The adaptive changes that occur in skeletal muscle with exercise training have been studied extensively, and various regulatory mechanisms have been identified.[3,7,8] The activation of p38 MAPK and PGC-1α have both been reported to mediate skeletal muscle adaptation to exercise training, but the specificities and sometimes contradictory observations have suggested underlying complexities, such as the importance of p38γ but not the α or β isoforms in exercise-induced mitochondrial biogenesis.[3,9,10] Skeletal muscle–specific overexpression of PGC-1α results in the expected shift toward slow-twitch fiber type; however, the muscle-specific PGC-1α knockout mouse still shows normal improvement in running capacity and fast-to slow-fiber transformation in response to exercise training.[11-13] Conflicting results have also been observed with the calcineurin-nuclear factor of activated T cells (NFAT) pathway in regulating muscle fiber types. Although one study found that neither calcineurin nor NFAT plays a dominant role in regulating slow-twitch fibers in adult skeletal muscle, other groups have shown that calcineurin-NFAT can induce slow fiber formation in response to muscle activity.[14-17] Acute exercise can also stimulate other signaling pathways in skeletal muscle such as the canonical pathway of NFKB, best known for its role in regulating innate immunity and inflammation.[18,19] NFKB has been found to be activated after treadmill exercise, suggesting a physiological role in muscle adaptation, as well in pathological conditions such as atrophy, and its noncanonical pathway has also been proposed to regulate myogenesis and mitochondrial biogenesis.[18,20-23] These disparate observations involving various signaling pathways highlight the complexities of skeletal muscle adaptation to exercise training and the need to further elucidate the molecular mechanisms underlying muscle homeostasis such as fiber type switching.

We previously observed that the coiled-coil-helix-coiled-coil-helix domain 4 (CHCHD4, mammalian homolog of yeast Mia40), a disulfide carrier involved in the active respiration-driven import of proteins into the intermitochondrial membrane space and thus critical for mitochondrial biogenesis,[24,25] was surprisingly downregulated in skeletal muscle by exercise-induced FOXO3.[26] Moreover, despite its high content of mitochondria, skeletal muscle showed the lowest level of CHCHD4 protein in a mouse tissue screen.[27] These apparently paradoxical observations suggested that CHCHD4 may serve additional functions beyond mitochondrial biogenesis in skeletal muscle such as those proposed for cancer cell hypoxia or neuronal cell survival signaling.[28,29] Here, we report that downregulation of CHCHD4 by exercise training can initiate a cascade of specific molecular events that result in the release of mtDNA into the cytosol and activation of innate immune signaling and NFKB, leading to increased oxidative slow fibers and the beneficial phenotype of decreased obesity with aging.

RESULTS

CHCHD4 overexpression prevents induction of oxidative type fibers in skeletal muscle by exercise training

To determine the physiological significance of CHCHD4 reduction by exercise training, we used CHCHD4 transgenic (Tg) mice, which have apparently normal development and lifespan.[26] At a young age (16 weeks old) CHCHD4 Tg mice did not appear significantly different from wild-type (WT) mice in terms of body weight or body mass index (Figures

S1A and S1B). The Tg mice showed a similar capacity for treadmill running compared with WT mice, but after 4 weeks of exercise training on a treadmill, WT mice ran significantly longer distances before exhaustion than CHCHD4 Tg mice (Figure 1A). In contrast to the WT mice, the CHCHD4 Tg mice did not exhibit an enhancement in exercise endurance following the same treadmill training regimen (Figure 1A). Similarly, following 4 weeks of access to voluntary wheel running with comparable utilization by both genotypes, the WT mice demonstrated a more significant improvement in maximal treadmill performance compared to the CHCHD4 Tg mice (Figures S1C and S1D). Consistent with the treadmill results, exercise training significantly increased the oxygen consumption (VO_2) of WT but not CHCHD4 Tg mice, as revealed by metabolic chamber measurements (Figure 1B). Mouse activity and feeding, which can affect VO_2, did not show a significant difference between WT and CHCHD4 Tg mice, with or without exercise training (Figure S2). These results suggested that exercise training significantly increases oxidative metabolism in WT but not CHCHD4 Tg mice. This was also in line with greater fat reduction in WT mice by exercise training after being fed a high-fat diet compared with Tg mice (Figure S3).

To obtain a comprehensive view of the molecular changes associated with CHCHD4 and exercise training, RNA sequencing (RNA-seq) data of skeletal muscles derived from both CHCHD4 Tg and WT mice, with or without exercise training, were subjected to principal-component analysis, which uncovered distinct differences among the four groups (Figure S4A). Gene Ontology enrichment analysis of the significantly changed genes showed that the top four pathways altered by CHCHD4 in exercise trained, but not unexercised, mice were related to muscle contractile function, suggesting a role for CHCHD4 in muscle adaptation (Figure S4B). As expected, RNA-seq profiling confirmed that CHCHD4 is highly expressed in CHCHD4 Tg mice compared with WT mice (Figure 1C; Tables S1-S3). Using volcano plots of gene expression ratios in the skeletal muscle of CHCHD4 Tg versus WT mice, MYH7, the myosin heavy chain expressed in oxidative slow-twitch type I fibers, stood out as one of the genes most significantly affected by exercise training. It shifted from the right side of the untrained sample plot (Figure 1C, left) to the left side of the trained sample plot (Figure 1C, right), indicating that training increases MYH7 expression more in WT mice than in CHCHD4 Tg mice. RT-PCR mRNA quantification of type I fiber MYH7 confirmed the RNA-seq data and showed that exercise training significantly increased the ratio of MYH7 to the glycolytic fast-twitch type IIb fiber MYH4 in the triceps surae muscle (comprising gastrocnemius, plantaris, and soleus) and tibialis anterior muscles of WT but not CHCHD4 Tg mice (Figures 1D and S5). The mRNA levels of the oxidative fast-twitch type IIa fiber MYH2 relative to MYH4 were also increased more in WT mice than in CHCHD4 Tg mice by exercise training, providing additional support for the involvement of CHCHD4 in reprogramming muscle metabolism (Figure 1D).

CHCHD4-regulated fiber formation is associated with MyoD levels

Examination of protein levels in the triceps surae muscle following exercise training showed that CHCHD4 was reduced to lower levels in WT mice than in CHCHD4 Tg mice as expected, whereas the levels of slow-twitch fiber troponin C (TnC, slow) isoform were increased more in WT mice than in CHCHD4 Tg mice by exercise training (Figure 1E). It was notable that the changes in slow TnC levels appeared to be inversely related to

CHCHD4 levels in both genotypes of mice, whereas the fast-twitch troponin C (TnC, fast) levels were correlated, helping to validate the observation (Figure 1E). The increased slow-twitch type I fibers in exercise-trained WT mice and the inhibition of this effect by CHCHD4 overexpression was further confirmed by MYH7 immunofluorescence and quantification in the triceps surae muscle (Figure 1F). In addition, the greater increases in the levels of the mitochondrial transcription factor A (TFAM) as a mitochondrial marker in WT compared with CHCHD4 Tg mice by exercise training correlated well with the changes in VO_2 and oxidative slow-twitch fibers (Figure 1E). Concomitantly, exercise training increased other mitochondrial proteins, such as those of complex IV and V, in the skeletal muscle of WT mice, whereas the increases were blunted in CHCHD4 Tg mice (Figure S6; Tables S4 and S5).

We next explored the possible mechanisms by which CHCHD4 may affect slow-twitch fiber formation after exercise training. PGC-1α was similarly induced by exercise training in both WT and CHCHD4 Tg mice, suggesting dissociated regulation of mitochondrial biogenesis from fiber type switching (Figure 1E). PGC-1β and calcineurin, both reported to play a role in fiber switching,[17,30] were not affected by CHCHD4 levels (Figure 1E). Consistent with a previous observation, calcineurin appeared to be slightly decreased by exercise training in both genotypes of mice.[31] However, MyoD, a major transcription factor that regulates myogenesis, was significantly decreased in exercise-trained WT mice, whereas this decrease was almost entirely prevented in CHCHD4 Tg mice (Figure 1E). Although initial studies showed that MyoD is not required for adult skeletal muscle development,[32] a subsequent study has reported that MyoD activity may play a role in facilitating skeletal muscle regeneration and regulating muscle fiber composition.[33] Furthermore, MyoD is known to be predominantly expressed in fast-twitch fibers, and its overexpression in muscle results in conversion from slow-to fast-twitch fibers, whereas MyoD knockout mice undergo the reverse process toward increased slow fibers.[34,35] Together, these data suggested that the downregulation of MyoD associated with CHCHD4 reduction plays an important role in the generation of slow-twitch fibers in response to exercise training.

TRIAP1 mediates CHCHD4 regulation of MyoD

To screen for molecules regulated by CHCHD4, we performed iTRAQ proteomic analysis of mitochondria purified from the skeletal muscle tissues of WT and CHCHD4 Tg mice. The protein (~8 kDa) encoded by *TP53-Regulated Inhibitor of Apoptosis 1* (*TRIAP1*) gene (also known as p53CSV), previously reported to require the disulfide relay for mitochondrial import in yeast (Mdm35),[36,37] was significantly increased in the Tg samples (Table S6). Conversely, TRIAP1 was identified as one of the proteins most decreased by CHCHD4 haploinsufficiency in a separate experiment using heart mitochondria from *CHCHD4* heterozygous knockout (*CHCHD4*$^{+/-}$) mice, which were previously reported to display no overt phenotype under normal conditions (Figure 2A).[38] The correlation between the levels of CHCHD4 and TRIAP1 by two independent proteomic analyses increased the likelihood of their specific interaction. *In vivo*, the levels of TRIAP1 decreased temporally following the decline of CHCHD4 in the skeletal muscle of WT mice after acute exercise, but this reduction in TRIAP1 was blocked by maintaining CHCHD4 levels in Tg mice (Figures 2B and 2C). Based on these observations, we hypothesized that TRIAP1 may be an interacting

protein that acts as a downstream mediator of CHCHD4 signaling for muscle fiber type switching.

To further demonstrate that it regulates TRIAP1 in muscle cells, CHCHD4 was overexpressed or knocked down in C2C12 myoblasts cultured in either regular growth or differentiation medium containing 2% horse serum for various periods of time and then processed for immunoblotting (Figures 2D and 2E). In control cells, TRIAP1 levels changed in a pattern similar to that of CHCHD4 after serum deprivation (Figures 2D and 2E). The decrease in TRIAP1 was accompanied by an increase in cleaved caspase-3, consistent with the known role of TRIAP1 as an inhibitor of apoptosis (Figures 2D and 2E). In contrast, CHCHD4 overexpression prevented the decrease in TRIAP1 levels and blocked the cleavage of caspase-3 during myoblast differentiation (Figure 2D). Interestingly, the overexpression of CHCHD4 also increased MyoD levels under both proliferating and differentiated states of the C2C12 myoblasts, consistent with the observation in skeletal muscle (Figure 2D). Conversely, CHCHD4 knockdown decreased TRIAP1 and MyoD levels while increasing cleaved caspase-3 levels (Figure 2E). Finally, knocking down TRIAP1 replicated the effects of CHCHD4 depletion by increasing cleaved caspase-3 and decreasing MyoD levels, indicating that TRIAP1 mediates the CHCHD4 regulation of MyoD (Figure 2F).

CHCHD4 and TRIAP1 regulate MyoD via the cGAS-STING-NFKB pathway

A number of studies have demonstrated that NFKB regulates MyoD expression and muscle myogenesis.[21] Chronic activation of NFKB leads to degradation of both mRNA and the protein of MyoD,[39,40] and in addition, a recent bioinformatic study identified TRIAP1 as a top candidate gene connected to the NFKB family of proteins using a gene expression dataset related to obesity.[41] In light of these findings, it was intriguing that TRIAP1 has been reported to form an intramitochondrial lipid transfer complex for the synthesis of cardiolipin (CL), a lipid that maintains the integrity of the inner mitochondrial membrane and prevents mtDNA release to trigger innate immune signaling.[42,43]

Acute exercise has previously been associated with mtDNA release in both mice and humans with the potential for innate immune signaling,[44-46] so we examined whether the downregulation of CHCHD4 and TRIAP1 would also activate NFKB by innate immune signaling with resultant MyoD degradation. Indeed, knockdown of CHCHD4 in C2C12 cells induced cGAS and promoted the activating phosphorylation of STING, IKKα/β, and NFKB subunit p65 while decreasing MyoD levels (Figure 3A). The specific reduction of TRIAP1 in mitochondria and the increased accumulation and DNA binding activity of p65 in the nucleus after CHCHD4 depletion were also confirmed (Figures 3B and 3C). Demonstrating its role as a mediator of this pathway, the direct knock down of TRIAP1 reproduced the activation of cGAS-STING and NFKB observed with CHCHD depletion (Figure 3D). Treatment with the STING inhibitor SN-011 blunted the phosphorylation of p65 induced by TRIAP1 knockdown, providing further evidence for cGAS-STING involvement in activating NFKB (Figure 3E).[47] Finally, knocking down p65 reversed the reduction of MyoD by TRIAP1 knockdown, indicating the essential role of NFKB in mediating the CHCHD4-TRIAP1 regulation of MyoD expression (Figure 3F).

CHCHD4-TRIAP1 induces VDAC oligomerization and mtDNA release to activate the cGAS-STING pathway

To further delineate the events triggering the observed innate immune signaling, we examined whether CHCHD4 depletion promotes mtDNA release from mitochondria. In C2C12 myoblasts, knockdown of either CHCHD4 or TRIAP1 induced mtDNA release into the cytoplasm, although the depletion of TRIAP1 as the downstream mediator of CHCHD4 may have contributed to the greater mtDNA release (Figure 4A). Mitochondrial VDAC oligomerization can form a channel for mtDNA release into cytosol, where the mtDNA can bind cGAS to activate the cGAS-STING innate immune signaling pathway.[48,49] Indeed, knocking down VDAC1 inhibited the release of mtDNA and cGAS-STING activation by TRIAP1 small hairpin RNA (shRNA) in C2C12 myoblasts (Figures 4A and 4B). Further confirming the role of VDAC in this pathway, treating TRIAP1 knockdown cells with VBIT4, which is known to bind VDAC and prevents its oligomerization, also reduced the cytosolic mtDNA levels and inhibited STING phosphorylation (Figures 4A and 4C).[50]

To further support the observation that mtDNA release mediates cGAS-STING signaling, mtDNA was depleted from C2C12 myoblasts by culturing in ethidium bromide (EtBr).[51] The EtBr-treated cells showed >80% mtDNA depletion with reduced respiration and increased glycolysis as expected (Figure S7). Knocking down CHCHD4 in these mtDNA-depleted cells failed to induce STING phosphorylation, indicating that mtDNA is required for activating this signaling pathway (Figure 4D). It is notable that the mtDNA-depleted cells showed increased CHCHD4 levels, which may be a feedback response for mitochondrial biogenesis due to respiratory insufficiency.

Increased VDAC dimerization in TRIAP1-depleted myoblasts was observed by treating the cells with graded concentrations of crosslinker ethylene glycolbis(succinimidylsuccinate) (EGS) followed by SDS-PAGE immunoblotting of VDAC (Figure 4E). TRIAP1 mediates the mitochondrial transport of phosphatidic acid for CL synthesis in the inner mitochondrial membrane.[42] CL is a unique, negatively charged lipid with four acyl chains that co-localizes with VDAC in the contact sites between the inner and outer mitochondrial membranes, and *in vitro* reconstitution experiments have shown that CL can prevent VDAC oligomerization.[52] Based on the finding that TRIAP1 is a substrate for CHCHD4, we examine using mass spectrometry whether CL species may be altered in the skeletal muscle of CHCHD4$^{+/-}$ and WT mice. The total level of CLs in *CHCHD4*$^{+/-}$ skeletal muscle was relatively unchanged compared to that of WT mice, but out of 50 CL species, 2 were significantly decreased in the skeletal muscle of *CHCHD4*$^{+/-}$ mice (Figure 4F; Table S7). The mature tetralinoleoyl-CL (CL 72:8), which is one of the most abundant and constitutes ~12% of the total CL, was lowered by ~30% in the *CHCHD4*$^{+/-}$ skeletal muscle. This mild reduction of a specific CL molecule could be sufficient to change VDAC dimerization. Indeed, there was increased dimerization of VDAC in *CHCHD4*$^{+/-}$ mitochondria detected by using either crosslinker/SDS-PAGE immunoblotting or native PAGE in the absence of crosslinker (Figures 4G and 4H). The fraction of oligomerized VDAC increased from ~10% in WT to ~20% in *CHCHD4*$^{+/-}$ mitochondria as determined by both methods (Figures 4G, 4H, and S8). In summary, these data suggested a model whereby the CHCHD4-TRIAP1 reduction in skeletal muscle by exercise training decreases specific CLs with subsequent

oligomerization of VDAC and release of mtDNA, causing cGAS-STING-NFKB-mediated downregulation of MyoD and increased slow-twitch fiber formation.

Haploinsufficiency of CHCHD4 mimics exercise training by activating innate immune signaling and increasing oxidative muscle fibers

Acute exercise has previously been found to activate NFKB signaling in muscle and thought to play a crucial role in muscle homeostasis and adaptation.[19] To test the *in vivo* role of CHCHD4 in innate immune signaling and NFKB activation, WT and CHCHD4 Tg mice were exercised and components of the innate immune signaling were assessed in their skeletal muscle during recovery (Figure 5A). The activating phosphorylation of STING and NFKB subunit p65 peaked at ~12 h after exercise in association with CHCHD4 reduction. These phosphorylations were largely blunted in CHCHD4 Tg mice, confirming the inhibitory role of CHCHD4 in this pathway *in vivo* (Figure 5A).

Because exercise causes a reduction in CHCHD4, we speculated that *CHCHD4*$^{+/-}$ mice may represent a genetic model of the exercise-trained state. Homozygous knockout *CHCHD4* (*CHCHD4*$^{-/-}$) mice have been reported to be embryonic lethal, whereas heterozygous *CHCHD4*$^{+/-}$ mice exhibit no overt phenotype, although interestingly they are resistant to weight gain with high-fat diet.[38] In *CHCHD4*$^{+/-}$ skeletal muscle, both CHCHD4 and TRIAP1 levels were reduced compared with that of WT mice, whereas there was increased phosphorylation of STING, IKKα/β, and p65, indicating activation of innate immune signaling (Figure 5B). Consistent with the results shown earlier, MyoD levels were significantly reduced in the *CHCHD4*$^{+/-}$ muscle samples, whereas MyoG, another member of the MyoD muscle transcription factor family that is essential for myofiber development, remained relatively unchanged (Figure 5B). Furthermore, the levels of TRIAP1 and phosphorylation of STING were either unchanged or undetectable in other tissues such as heart, lung, liver, brain, and spleen of *CHCHD4*$^{+/-}$ mice, suggesting tissue-specific regulation of this pathway (Figure S9). In line with this observation, there was no evidence of diffuse systemic inflammation associated with CHCHD4 deficiency as measured by plasma cytokine profiling (Figure S10). Aged *CHCHD4*$^{+/-}$ mice appeared healthy and, in fact, although not statistically significant, their median lifespan was slightly longer than that of either WT or CHCHD4 Tg mice (*CHCHD4*$^{+/-}$, 770 days; WT, 739 days; CHCHD4 Tg, 732 days) (Figure S11).

Reflecting an exercise-trained state, quantification of skeletal muscle proteins by immunoblotting showed that in addition to increased activation of NFKB subunit p65 and reduced MyoD, the ratio of slow to fast TnC was significantly increased in *CHCHD4*$^{+/-}$ mice compared with WT (Figure 5C). The mRNA ratio of slow type I (MYH7) to fast type IIb (MYH4) fiber was also significantly increased in the skeletal muscle of *CHCHD4*$^{+/-}$ mice, whereas the ratio of oxidative fast type IIa (MYH2) to MYH4 showed a trend of increase (Figure 5C). Furthermore, immunofluorescence revealed stronger slow fiber MYH7^{+} signals in both the lateral and medial heads of the gastrocnemius muscle of *CHCHD4*$^{+/-}$ mice compared with that of WT mice (Figures 5D, 5E, and S12). Therefore, similar to MyoD-deficient mice,[34] *CHCHD4*$^{+/-}$ mice displayed a switch from fast-to slow-twitch fibers in their skeletal muscle (i.e., from glycolytic to oxidative fibers), supporting a

role for the CHCHD4-innate immune signaling pathway in MyoD regulation. Consistently, we also observed increased levels of the oxidative fast fiber type IIa in the plantaris muscle of *CHCHD4*$^{+/-}$ mice (Figure 5F). However, no significant difference in the glycolytic fast-twitch type IIb fibers, distinguished by large diameters, was noted among the three genotypes (Figure S13).

To further characterize the exercise training–associated phenotype of *CHCHD4*$^{+/-}$ mice, whol-body metabolic measurements were performed, but no significant differences could be detected when comparing heterozygous with WT mice (Figure S14). However, metabolomic profiling of the triceps surae muscle identified three significantly changed metabolites in *CHCHD4*$^{+/-}$ mice compared with WT mice. β-Hydroxybutyric acid (BHB) topped the list with a tissue concentration decrease of 40% in *CHCHD4*$^{+/-}$ mice (Figure 5G; Table S8). Measuring BHB revealed that its level was unchanged in liver but decreased in plasma of *CHCHD4*$^{+/-}$ mice compared with that of WT mice, suggesting increased consumption of BHB by the peripheral tissues of *CHCHD4*$^{+/-}$ mice (Figure S15). BHB, a ketone body generated in liver, is mainly used by skeletal muscle mitochondria after transport across the plasma membrane via the mono-carboxylate transporter 1 (MCT1). MCT1 is known to be predominantly expressed in slow-twitch type I fibers as well as in exercise-trained skeletal muscles, with increased capacity for ketone body uptake.[53] The higher basal levels of MCT1 in the skeletal muscle of *CHCHD4*$^{+/-}$ mice suggested a genetically determined exercise-trained state (Figure 5B). In addition, metabolomic profiling showed lower levels of cytidine and uridine in the skeletal muscle of *CHCHD4*$^{+/-}$ mice, suggesting alteration of pyrimidine metabolism, which has been linked to skeletal muscle fiber type switching and mitochondrial biogenesis.[54]

Haploinsufficiency of CHCHD4 confers beneficial effects of exercise training

The increased oxidative fibers observed in *CHCHD4*$^{+/-}$ skeletal muscle were further substantiated by the higher basal levels of the mitochondrial biogenesis factors PGC1α, PGC1β, and TFAM but not phospho-p38 (Figures 6A and 6B). *CHCHD4*$^{+/-}$ skeletal muscle also showed higher mtDNA content than that of WT, mirroring the increased levels of TFAM, which is important for mtDNA homeostasis (Figure 6B). Despite the decreased levels of the cell survival factor TRIAP1, the level of apoptosis as indicated by cleaved caspase-3 was not increased in the skeletal muscle of *CHCHD4*$^{+/-}$ mice. Notably, however, the autophagy marker LC3-II was increased, pointing to the possibility of mitophagy activation (Figures 6A and 6B).

To assess the role of CHCHD4 on mitophagy, mt-Keima mice, which permit detection of *in vivo* mitophagy, were crossed with *CHCHD4*$^{+/-}$ or CHCHD4 Tg mice, and their skeletal muscles were imaged by fluorescence microscopy (Figure 6C).[55] After 60 min of treadmill exercise, the increase in the red:green ratio of mt-Keima in the skeletal muscle of *CHCHD4*$^{+/-}$ compared with WT mice became significant (Figures 6C and 6D). In contrast, the overexpression of CHCHD4 in Tg mice blunted the increase in mt-Keima signal. These results indicated that *CHCHD4*$^{+/-}$ mice have increased mitophagy in their skeletal muscle, which, in conjunction with mitochondrial biogenesis, may play an important role in exercise adaptation.[56,57]

Ex vivo tissue metabolism of skeletal muscle was also measured using Seahorse XF24 Analyzer, as described previously.[58] Compared with WT mice, *CHCHD4*$^{+/-}$ mice showed an increased oxygen consumption rate (OCR), whereas CHCHD4 Tg mice displayed decreased OCR in soleus muscle, which contains predominantly slow-twitch fibers enriched in mitochondria with fatty acid oxidizing potential (Figure 7A). Plantaris muscle, which is composed of mixed fibers, showed lower OCR values than soleus as expected, but the effect of CHCHD4 on respiration remained (Figure 7A).

With similar levels of exercise training using voluntary wheels, *CHCHD4*$^{+/-}$ mice also showed a greater improvement in treadmill running capacity compared with WT mice (68% versus 58%, respectively) (Figures 7B and S16). This observation in CHCHD4 haploinsufficient mice contrasted with the lack of improvement upon exercise training in CHCHD4 overexpressing Tg mice (Figure 1A). Compared with WT mice, *CHCHD4*$^{+/-}$ mice showed less increase in blood lactate levels (37% versus 90%) after submaximal exercise testing, possibly due to higher oxidative muscle fiber levels and lower anaerobic metabolism (Figure 7C). In line with a previous report that *CHCHD4*$^{+/-}$ mice are resistant to weight gain when fed a high-fat diet,[38] CHCHD4 haploinsufficient mice gained significantly less weight compared with WT mice as they aged to 52 weeks, although their weights were initially similar when younger (16 weeks) (Figure 7D). In contrast to WT and CHCHD4 Tg mice, which showed increased fat and decreased lean mass with aging (52 weeks), *CHCHD4*$^{+/-}$ mice displayed the beneficial exercise training–associated pattern of lower fat and higher lean mass (Figures 7E and S1B). These metabolic and body mass index data were consistent with the mitochondrial respiration measurements in skeletal muscles (Figure 7A).

Further supporting these results, the RNA-seq data indicated that downregulation of CHCHD4 in skeletal muscle could contribute to the beneficial molecular changes induced by exercise training. Exercise training increased the expression of *MT-ND3* and *ATP1A3* as markers of mitochondrial biogenesis in WT, but not CHCHD4 Tg, mice (Tables S4 and S5). The RNA-seq analysis also identified the increased expression of several other genes, such as *RRAD*, *PLAC8*, and *CIDEA* in association with slow fiber *MYH7*, whose activities would be expected to be increased by exercise training in WT, but not CHCHD4 Tg, mice (Tables S4 and S5). RRAD inhibits glycolysis,[59] PLAC8 promotes autophagy,[60] and CIDEA enhances insulin sensitivity.[61] Thus, CHCHD4 downregulation may play a role in the signaling pathways regulating the various beneficial metabolic changes associated with exercise training.

DISCUSSION

After reporting on the initial observation of decreased CHCHD4 levels by exercise stimulation in skeletal muscle,[26] we have now uncovered an exercise adaptation mechanism in which this mitochondrial protein import carrier CHCHD4 can regulate mtDNA release into the cytosol through VDAC oligomerization, thereby triggering the cGAS-STING-NFKB pathway for muscle fiber type switching via MyoD (Figure 7F). Although the observations of NFKB activation by innate immune signaling, MyoD regulation by NFKB, and oxidative slow-twitch fiber type modulation by MyoD have been described separately,[39,40,62-64] our current work on the role of CHCHD4 in exercise adaptation

provides a framework for integrating these molecular mediators into a signaling pathway for fiber type switching. An interesting feature of this mechanism is its dynamic nature, whereby the critical signal mediator TRIAP1 is a substrate of the carrier CHCHD4, which in turn is dependent on mitochondrial respiration for its protein import activity. It is tempting to speculate that such a functionally driven signaling mechanism may be well suited for the complexities of skeletal muscle adaptation to exercise training.[1,3,7,8] For example, it may permit the homeostatic setting of fiber type transition to be continuously variable, depending on, for example, the functional state of the muscle cell and mitochondria.[65]

Our study also demonstrates that exercise training–mediated skeletal muscle fiber type switching is mediated by sublethal stress signaling from the mitochondrion involving the innate immune response. This is accomplished by the CHCHD4-mediated import of TRIAP1 into the mitochondria that in turn determines the levels of CL, critical for maintaining the integrity of the inner mitochondrial membrane and preventing mtDNA release into the cytosol. Although exercise-induced NFKB can have a positive effect on mitochondrial and myogenesis,[19,21] the overactivation of NFKB can also cause skeletal muscle atrophy.[39,66] Thus, NFKB regulation of MyoD and slow-twitch fiber switching may be a double-edged sword with respect to muscle atrophy or adaptation via, for example, the degree of VDAC oligomerization and mtDNA release. The level of constitutive innate immune activation in the skeletal muscle of *CHCHD4*$^{+/-}$ mice is sufficient to increase the composition of slow-twitch fibers in their skeletal muscle without causing systemic inflammation or shortening of lifespan (Figure S11).

Exercise training can lead to structural and metabolic remodeling of skeletal muscle, characterized by an increase in oxidative slow-twitch fibers, which play a role in preventing obesity, type 2 diabetes, and cardiovascular diseases.[3] According to a long-term follow-up study, men with different proportions of type I fiber in their skeletal muscle had similar body mass indices when young. However, those with low levels of type I fiber gained an average of ~13 kg more weight than those with high levels in their later years.[6] As observed in this human study, *CHCHD4*$^{+/-}$ mice with higher levels of type I fibers in their skeletal muscle had less weight gain and lower body fat composition with aging, which is further supported by a previous report that these mice are resistant to weight gain while on a high-fat diet.[38] Thus, our study suggests that modulating the innate immune signaling elicited from mitochondria by CHCHD4 could be used as a therapeutic strategy for preventing obesity and improved glucose homeostasis. Finally, it may be interesting to explore whether exercise-induced innate immune signaling, which promotes type I fibers, also contributes to modulating the immune system, for example, in conditions such as autoimmune diseases.

Limitations of the study

We used genetic mouse models with global overexpression of CHCHD4 or its haploinsufficiency to investigate the role of exercise-regulated CHCHD4 in muscle fiber homeostasis and its contribution to health. Although we identified a specific innate immune signaling pathway in myoblast and skeletal muscle that can regulate muscle fiber composition, the contributory effect of other cell types or tissues on our observation cannot be ruled out. In addition, exercise activates other signaling pathways that could affect

muscle composition and function. Indeed, our RNA-seq analysis of skeletal muscle showed that CHCHD4 levels can affect the expression of genes important for processes such as mitochondrial biogenesis, autophagy, and insulin sensitivity. Thus, exercise regulation of CHCHD4 may have other activities that promote healthy metabolism and warrants further investigation.

STAR★METHODS

RESOURCE AVAILABILITY

Lead contact—Further information and requests for reagents may be directed to and will be fulfilled by the Lead Contact, Paul M Hwang (hwangp@mail.nih.gov).

Materials availability—Unique reagents generated in this study will be made available under a standard material transfer agreement on request from the lead contact.

Data and code availability

- The RNA-seq analysis data have been deposited to the Gene Expression Omnibus (GEO) under the dataset identifier: GSE245760. Additionally, the Cardiolipin Analysis, Metabolome Analysis, and iTRAQ datasets have been deposited in the Fig-share with the dataset identifier: https://doi.org/10.25444/nhlbi.24402901.
- This paper does not report original code.
- Any additional information required to reanalyze the data reported in this paper is available from the lead contact upon request.

EXPERIMENTAL MODEL AND STUDY PARTICIPANT DETAILS

Mouse models—All mice used in this study were maintained and handled in accordance with the NHLBI Animal Care and Use Committee protocol. Wild-type, *CHCHD4*$^{+/-}$ (Texas A&M Institute for Genomic Medicine) and CHCHD4 transgenic (Tg) mice were of the C57BL/6 background strain. To express CHCHD4 ubiquitously in mice, a full-length mouse CHCHD4 cDNA (untagged) was subcloned into pBROAD3 vector (InvivoGen, San Diego, CA), which contains the mouse ROSA26 promoter and the rabbit β-globin polyadenylation sequence.[26] mt-Keima transgenic mice (strain FVB/NJ) were a kind gift from Toren Finkel (University of Pittsburgh).[55] Tail DNA was used for standard PCR or quantitative real-time PCR for *CHCHD4*$^{+/-}$ or CHCHD4 Tg mouse genotyping, respectively (see Table S9, primer sequences). Male mice (10–52 wk old) were used for experiments.

Cell culture—Mouse C2C12 cell lines were obtained from ATCC and cultured in DMEM medium supplemented with 10% FBS. To induce myogenic differentiation, the growth medium was switched to differentiation medium (DMEM supplemented with 2% horse serum, Sigma) once myoblasts had reached over 90% confluency. Myoblast cells were either harvested at 90% confluency or allowed to mature into myotubes for 1, 3 or 10 d before being harvested. STING antagonist SN-001 (cat. # 34890, Cayman, Inc) and VDAC

oligomerization inhibitor VBIT-4 (cat. # AOB8202, AOBIOUS) were solubilized in DMSO prior to their use at the indicated final concentration.

METHOD DETAILS

Mouse metabolic studies—For the high-fat diet study, mice were fed a rodent diet with 60 kcal% fat (cat. #D12492, Research Diets) for 8 wk. After the 8 wk period, the mice were switched to a normal diet with or without exercise training for an additional 4 wk during which time body measurements were made. The body composition of non-anesthetized mice was measured using the Minispec NMR analyzer (Bruker). While monitoring food intake and activity, metabolism was measured in the mice by indirect calorimetry (O_2 consumption and CO_2 production) using a Comprehensive Lab Animal Monitoring System (Oxymax/CLAMS, Columbus Instruments, OH).

Mouse exercise training, treadmill running test and blood lactate measurement—For voluntary running exercise training, mice were housed in individual cages equipped with a monitored running wheel apparatus for the specified time, allowing quantification of their running levels (Med Associates Inc). Treadmill exercise training and maximal running capacity test were performed as previously described protocols.[67] Sub-maximal exercise was performed on a treadmill by starting at 12 m/min with incremental speed increases of 2 m/min every 3 min and stopped after 22 min, corresponding to ~70% maximal running capacity. Tail blood lactate levels were measured before and after treadmill exercise using a Lactate Pro Analyzer (Arkray).

Gene knockdown and overexpression—The plasmids used in this study were as follows: mouse CHCHD4 shRNA in pGIPZ (RMM4431-200361800) and control vector (RHS4348) (Horizon Discovery); mouse CHCHD4 cDNA in pReceiver-Lv105 (EX-Mm10785-Lv105) and control vector (EXNEG-Lv105); mouse VDAC1 shRNA in psi-LVRH1H (MSH096502-LVRU6P) and control vector (CSHCTR001-LVRU6P) and mouse TRIAP1 shRNA in psi-LVRH1H (MSH034752-LVRH1H) and control vector (CSHCTR001-LVRH1H) (GeneCopoeia). Lentiviruses for overexpression and knockdown experiments were prepared using the MISSION Lentiviral Packaging Mix according to manufacturer's instructions (SHP001, Sigma-Aldrich). Cells were transduced with lentivirus for 24 h, followed by selection with 2 μg/mL puromycin (for CHCHD4 shRNA and Cdna; VDAC1 shRNA) or hygromycin B 500 μg/mL (for TRIAP1 shRNA). Transient transfections were carried out using Fugene HD transfection reagent (Roche).

Protein immunoblotting—Proteins were separated by Tris-Glycine SDS-PAGE and detected by immunoblotting using standard ECL Plus Western Blotting Substrate (Pierce). ChemiDoc Tough Imaging System (Bio-Rad) was used to visualize and quantify the chemiluminescent intensity of protein bands. Antibodies are listed in the key resources table.

Tissue and cell subcellular fractionation—Skeletal muscle (gastrocnemius unless indicated otherwise) was harvested from hindlimbs of mice before and after exercise training. Mitochondria from heart and skeletal muscle were purified using standard centrifugation technique as previously described.[68] C2C12 mouse myoblasts were harvested

and subcellularly fractionated using a previously described method.[69] Briefly, cells were homogenized in fractionation buffer (200 mM sucrose, 50 mM Tris- HCl pH 7.4, 5 mM MgCl2) using a tissue grinder and centrifuged at 800x g for 15 min. The resulting pellet and supernatant were used to isolate the nuclear and cytosolic fractions, respectively. The pellet was resuspended in RIPA buffer and centrifuged at 12,000x g for 30 min to yield the soluble nuclear fraction in the resulting supernatant. The initial supernatant was centrifuged at 12,000x g for 10 min to yield the cytosolic fraction in the resulting supernatant.

Muscle immunofluorescence imaging—The gastrocnemius muscle was oriented for cross-section imaging, immobilized with gum tragacanth (cat. # SLCF9027, Sigma-Aldrich) before being snap-frozen in isopentane cooled in liquid nitrogen. Sections (10 μm) of transversely-oriented muscle were cut on a Leica Cryomicrotome at −20°C, and the sections from the mid-part of each muscle were used. The tissue sections were allowed to attach and dry to slides at room temperature for 30 min, fixed in 1% paraformaldehyde (Santa Cruz) PBS, and permeabilized in 0.1% Triton X-100 PBS. Immunofluorescent labeling was performed by blocking with 5% serum (of the secondary antibody species) at room temperature, followed by incubating with primary anti-MYH7 (MHC1) antibody (BA-D5, DSHB), anti-MYH4 (MHC), anti-MYH2(MHC) at 4°C overnight. The sample was then then incubated with Alexa Fluro488-labeled secondary antibody (Invitrogen) at 37°C for 1 h. PBS washes were performed between all steps, and images were captured using a Zeiss LSM 780 confocal microscope. Quantification was performed using ImageJ software.

RNA quantification by real-time RT-PCR—Tissue RNA was purified using the RNeasy kit (Qiagen) and used to synthesize doublestranded cDNAs using SuperScript Double-Stranded cDNA Synthesis Kit (Thermo Fisher Scientific). Real-time RT-PCR was performed using an ABI HT7900 thermal cycler as previously described.[70] mRNA expression was measured by calculating the average cycle threshold (Ct) ratio relative to the housekeeping gene *TIF.*

RNA-seq analysis—RNA samples were used to synthesize double-stranded cDNAs using SuperScript DoubleStranded cDNA Synthesis Kit (Thermo Fisher Scientific). The sequencing and data analysis were performed by the NHLBI DNA Sequencing and Genomics Core. Raw data files (FASTQ format) were aligned to the Mouse GENCODE Gene Set (Release M25) using STAR/2.7.8a with default parameters, and the expected counts were quantified using RSEM/1.3.2. This work utilized the computational resources of the NIH HPC Biowulf cluster (http://hpc.nih.gov). Differentially analysis were performed using the edgeR exactTest function. Isobaric Tags for Relative and Absolute Quantitation (iTRAQ) proteomics analysis Using purified mitochondria, 100 μg protein/channel in 8 M urea were prepared. The isobaric tags for relative and absolute quantitation were analyzed by performing LCMS on a Thermo Orbitrap Lumos-based nanoLCMS system by the NHLBI Proteomics Core. The data were analyzed using the Thermo Proteome Discoverer 2.4 Platform (PD 2.4).

Metabolomic analysis—The metabolites in mouse gastrocnemius muscle were analyzed using both capillary electrophoresis time-of-flight mass spectrometry (CE-TOFMS)

and liquid chromatography time-of-flight mass spectrometry (LC-TOFMS) by Human Metabolome Technologies, Inc (Boston).

Cardiolipin analysis—The cardiolipins in mouse gastrocnemius muscle tissues were analyzed using Waters' Xevo TQ-S tandem quadrupole mass spectrometer by Creative Proteomics, Inc. (New York).

Quantification of mtDNA release—mtDNA release into the cytosol from mitochondria was quantified using a modified protocol as previously described.[71] Samples of C2C12 cells (5×10^6) were divided into 2 aliquots (each containing 2.5×10^6 cells). One aliquot was used to extract whole cell DNA (containing total mtDNA) with DNeasy Blood & Tissue Kit (Qiagen) while the other was resuspended in 200 μL of permeabilization buffer (150 mM NaCl, 50 mM HEPES pH 7.4, and 25 μg/mL digitonin (Tokyo Chemical Industry)) for isolating cytosolic mtDNA. Specifically, the resuspended cell sample was incubated on a rotator at room temperature for 10 min, and then centrifuged at 16,000x g at 4°C for 25 min to collect the supernatant containing the cytosolic mtDNA. Quantitative real-time PCR was then performed on the supernatant (cytosolic mtDNA) and the whole-cell DNA (total mtDNA) utilizing primers specific for mtDNA (*MT-ND1)* and nuclear DNA (*18S rRNA*) as internal control. The cycle threshold (Ct) value of *MT-ND1* was normalized using the Ct value of *18S rRNA* to calculate the relative mtDNA copy number. To quantify mtDNA release, the copy number of cytosolic mtDNA was divided by that of total mtDNA.

VDAC oligomerization assay—C2C12 cells were harvested in PBS, and a small fraction hypotonic lysed for protein concentration measurement. Cells in PBS with a protein concentration of 2.5–3 mg/mL were incubated with cross-linking reagent ethylene glycol bis (succinimidyl succinate) (EGS) (cat. #C1130, ProteoChem) at a concentration of 100–300 μM at 30°C for 20 min. Skeletal muscle mitochondria at a concentration of 1 mg/mL was also incubated with 150 μM EGS at 30°C for 20 min. After the treatment, the cells or mitochondria were spun down and dissolved in RIPA buffer. The solubilized proteins were quantified and separated by Tris-Glycine SDS-PAGE, then immunoblotted using anti-VDAC1 monoclonal antibody.[48,49] In addition, purified mitochondria were solubilized in NativePAGE sample buffer (Invitrogen) containing 1% digitonin and 1% Triton X-100 at 4°C for 1 h and then centrifuged at 20,000x g for 20 min. Approximately 10 μg of protein from the supernatant were resolved in a 4–16% gradient NativePAGE Novex Bis-Tris gel and transferred to immobilon-PVDF membrane. The membrane was then immunoblotted by VDAC1 antibody to detect VDAC1 complex by ECL. ChemiDoc Tough Imaging System (Bio-Rad) was used to visualize and quantify the chemiluminescent intensity of the protein bands.

NFKB transactivation assay—The NFKB (p65) DNA-binding activity was measured using the NFKB Transcription Factor Assay kit (cat. # 10007889, Cayman Chemical) according to the manufacturer's instructions. Briefly, nuclear extracts of cells were prepared using the method described above, and equal amounts of nuclear extracts were loaded to coated wells containing a specific double-stranded DNA sequence with the NFKB response element. Primary antibody directed against NFKB and secondary antibody conjugated to

HRP were added and incubated for 1 h. The developing solution was added, and the absorbance was measured at 450 nm using a Synergy H1 microplate reader (Biotech Instruments, Inc).

Mouse cytokine array—The mouse cytokine array analysis was performed using the R&D Systems Mouse Cytokine Array Kit (cat. # ARY006) according to the manufacturer's instructions. Freshly collected plasma (200 μL) was mixed with a cocktail of biotinylated detection antibodies and then incubated with an array membrane that contained duplicate spots of capture antibodies to the specific targets. The captured proteins were then visualized using chemiluminescent detection reagents and imaged using the same method as described for immunoblotting.

Mt-Keima mitophagy imaging—*In vivo* mitophagy were visualized using mt-Keima mouse tissue as previously described.[72] Briefly, the plantaris skeletal muscle was rinsed with cold PBS and placed on 35-mm cover glass #1.5-bottom micro-well plates (MatTek) for immediate analysis. Samples were imaged on a Zeiss LSM 780 confocal microscope in 2 channels by 2 sequential excitations (458 nm, green; 561 nm, red) using 570 to 695 nm emission range (Carl Zeiss MicroImaging). Quantification of mitophagy was performed using Zeiss ZEN software on a pixel-by-pixel basis as previously described.[55] Briefly, every pixel in the image is plotted on the scatter diagram based on its intensity level from each channel. The x and y axes represent green and red signals, respectively. Relative mt-Keima signal was quantified by the number of pixels that have high red intensity over the number of all pixels. The average values of the controls were assigned as 1. In each experiment, all parameters remained the same for acquiring all imaging data.

***Ex vivo* whole muscle metabolic assay—**For measuring *ex vivo* muscle oxidative metabolism, whole soleus and plantaris muscles were dissected and embedded on islet capture microplates. Their oxygen consumption rate based on the utilization of endogenous substrates was measured.[58]

β-hydroxybutyrate assay—β-hydroxybutyrate levels in tissues and plasma were measured using the beta Hydroxybutyrate Assay Kit (cat.# ab83390, ABCAM) according to the manufacturer's instructions. For liver samples, 20 mg of tissue was harvested, washed in PBS, and suspended in 100 μL of assay buffer. The tissues were homogenized on ice, centrifuged at 20,000x g in 4°C for 5 min, and the resulting supernatants were subjected to perchloric acid (PCA) precipitation to eliminate interfering proteins. Plasma samples were deproteinized using a 10 kD Spin Column (cat.# ab93349, ABCAM), assayed and measured using a microplate reader (450 nm).

QUANTIFICATION AND STATISTICAL ANALYSIS

Quantification of western blots was performed using ImageJ software.

Statistical analysis was performed using GraphPad Prism software (version 7). One-way ANOVA, two-way ANOVA, and two-tailed unpaired *t*-tests were used to compare the data with corresponding controls. Metabolomic data were performed using MetaboAnalyst 3.0 (https://www.metaboanalyst.ca/).[73]

Supplementary Material

Refer to Web version on PubMed Central for supplementary material.

ACKNOWLEDGMENTS

We thank past members of our laboratory, in particular, William M. Kamp and Ju-Gyeong Kang, and are grateful to Nuo Sun (Ohio State University) and Toren Finkel (University of Pittsburgh) for advice/assistance and the kind gift of the mt-Keima mouse. We also thank Chengyu Liu (Transgenic Core), Audrey C. Noguchi, Heather Potts and Danielle A. Springer (Murine Phenotyping Core), Katherine Pak (National Institute of Arthritis and Musculoskeletal and Skin Diseases, NIH), Zu-Xi Yu (National Heart, Lung, and Blood Institute [NHLBI] Pathology Facility), Yuesheng Li (NHLBI DNA Sequencing and Genomics Core), Christian A. Combs (NHLBI Light Microscopy Core), and Guanghui Wang and Marjan Gucek (NHLBI Proteomics Core Facility) for helpful advice and assistance during the course of this study. This work was supported by the NHLBI-NIH Division of Intramural Research (HL006051) (to P.M.H.).

REFERENCES

1. Baskin KK, Winders BR, and Olson EN (2015). Muscle as a "mediator" of systemic metabolism. Cell Metab. 21, 237–248. [PubMed: 25651178]
2. Schiaffino S, and Reggiani C (2011). Fiber Types in Mammalian Skeletal Muscles. Physiol. Rev 91, 1447–1531. [PubMed: 22013216]
3. Egan B, and Zierath JR (2013). Exercise metabolism and the molecular regulation of skeletal muscle adaptation. Cell Metab. 17, 162–184. [PubMed: 23395166]
4. Wade AJ, Marbut MM, and Round JM (1990). Muscle fibre type and aetiology of obesity. Lancet 335, 805–808. [PubMed: 1969558]
5. Tanner CJ, Barakat HA, Dohm GL, Pories WJ, MacDonald KG, Cunningham PRG, Swanson MS, and Houmard JA (2002). Muscle fiber type is associated with obesity and weight loss. Am. J. Physiol. Endocrinol. Metab 282, E1191–E1196. [PubMed: 12006347]
6. Karjalainen J, Tikkanen H, Hernelahti M, and Kujala UM (2006). Muscle fiber-type distribution predicts weight gain and unfavorable left ventricular geometry: a 19 year follow-up study. BMC Cardiovasc. Disord 6, 2. [PubMed: 16403232]
7. Yan Z, Okutsu M, Akhtar YN, and Lira VA (2011). Regulation of exercise-induced fiber type transformation, mitochondrial biogenesis, and angiogenesis in skeletal muscle. J. Appl. Physiol 110, 264–274. [PubMed: 21030673]
8. Hawley JA, Hargreaves M, Joyner MJ, and Zierath JR (2014). Integrative biology of exercise. Cell 159, 738–749. [PubMed: 25417152]
9. Akimoto T, Pohnert SC, Li P, Zhang M, Gumbs C, Rosenberg PB, Williams RS, and Yan Z (2005). Exercise stimulates Pgc-1alpha transcription in skeletal muscle through activation of the p38 MAPK pathway. J. Biol. Chem 280, 19587–19593. [PubMed: 15767263]
10. Pogozelski AR, Geng T, Li P, Yin X, Lira VA, Zhang M, Chi JT, and Yan Z (2009). p38gamma mitogen-activated protein kinase is a key regulator in skeletal muscle metabolic adaptation in mice. PLoS One 4, e7934. [PubMed: 19936205]
11. Lin J, Wu H, Tarr PT, Zhang CY, Wu Z, Boss O, Michael LF, Puigserver P, Isotani E, Olson EN, et al. (2002). Transcriptional coactivator PGC-1 alpha drives the formation of slow-twitch muscle fibres. Nature 418, 797–801. [PubMed: 12181572]
12. Handschin C, Chin S, Li P, Liu F, Maratos-Flier E, Lebrasseur NK, Yan Z, and Spiegelman BM (2007). Skeletal muscle fiber-type switching, exercise intolerance, and myopathy in PGC-1alpha muscle-specific knock-out animals. J. Biol. Chem 282, 30014–30021. [PubMed: 17702743]
13. Geng T, Li P, Okutsu M, Yin X, Kwek J, Zhang M, and Yan Z (2010). PGC-1alpha plays a functional role in exercise-induced mitochondrial biogenesis and angiogenesis but not fiber-type transformation in mouse skeletal muscle. Am. J. Physiol. Cell Physiol 298, C572–C579. [PubMed: 20032509]

14. Chin ER, Olson EN, Richardson JA, Yang Q, Humphries C, Shelton JM, Wu H, Zhu W, Bassel-Duby R, and Williams RS (1998). A calcineurin-dependent transcriptional pathway controls skeletal muscle fiber type. Genes Dev. 12, 2499–2509. [PubMed: 9716403]
15. Delling U, Tureckova J, Lim HW, De Windt LJ, Rotwein P, and Molkentin JD (2000). A calcineurin-NFATc3-dependent pathway regulates skeletal muscle differentiation and slow myosin heavy-chain expression. Mol. Cell Biol 20, 6600–6611. [PubMed: 10938134]
16. Swoap SJ, Hunter RB, Stevenson EJ, Felton HM, Kansagra NV, Lang JM, Esser KA, and Kandarian SC (2000). The calcineurin-NFAT pathway and muscle fiber-type gene expression. Am. J. Physiol. Cell Physiol 279, C915–C924. [PubMed: 11003571]
17. Schulz RA, and Yutzey KE (2004). Calcineurin signaling and NFAT activation in cardiovascular and skeletal muscle development. Dev. Biol 266, 1–16. [PubMed: 14729474]
18. Ji LL, Gomez-Cabrera MC, Steinhafel N, and Vina J (2004). Acute exercise activates nuclear factor (NF)-kappaB signaling pathway in rat skeletal muscle. FASEB J. 18, 1499–1506. [PubMed: 15466358]
19. Kramer HF, and Goodyear LJ (2007). Exercise, MAPK, and NF-kappaB signaling in skeletal muscle. J. Appl. Physiol 103, 388–395. [PubMed: 17303713]
20. Ho RC, Hirshman MF, Li Y, Cai D, Farmer JR, Aschenbach WG, Witczak CA, Shoelson SE, and Goodyear LJ (2005). Regulation of IkappaB kinase and NF-kappaB in contracting adult rat skeletal muscle. Am. J. Physiol. Cell Physiol 289, C794–C801. [PubMed: 15888549]
21. Bakkar N, and Guttridge DC (2010). NF-kappaB signaling: a tale of two pathways in skeletal myogenesis. Physiol. Rev 90, 495–511. [PubMed: 20393192]
22. Bakkar N, Ladner K, Canan BD, Liyanarachchi S, Bal NC, Pant M, Periasamy M, Li Q, Janssen PML, and Guttridge DC (2012). IKKalpha and alternative NF-kappaB regulate PGC-1beta to promote oxidative muscle metabolism. J. Cell Biol 196, 497–511. [PubMed: 22351927]
23. Thoma A, and Lightfoot AP (2018). NF-kB and Inflammatory Cytokine Signalling: Role in Skeletal Muscle Atrophy. Adv. Exp. Med. Biol 1088, 267–279. [PubMed: 30390256]
24. Riemer J, Fischer M, and Herrmann JM (2011). Oxidation-driven protein import into mitochondria: Insights and blind spots. Biochim. Biophys. Acta 1808, 981–989. [PubMed: 20537978]
25. Al-Habib H, and Ashcroft M (2021). CHCHD4 (MIA40) and the mitochondrial disulfide relay system. Biochem. Soc. Trans 49, 17–27. [PubMed: 33599699]
26. Zhuang J, Kamp WM, Li J, Liu C, Kang JG, Wang PY, and Hwang PM (2016). Forkhead Box O3A (FOXO3) and the Mitochondrial Disulfide Relay Carrier (CHCHD4) Regulate p53 Protein Nuclear Activity in Response to Exercise. J. Biol. Chem 291, 24819–24827. [PubMed: 27687729]
27. Hofmann S, Rothbauer U, Mühlenbein N, Baiker K, Hell K, and Bauer MF (2005). Functional and mutational characterization of human MIA40 acting during import into the mitochondrial intermembrane space. J. Mol. Biol 353, 517–528. [PubMed: 16185709]
28. Yang J, Staples O, Thomas LW, Briston T, Robson M, Poon E, Simões ML, El-Emir E, Buffa FM, Ahmed A, et al. (2012). Human CHCHD4 mitochondrial proteins regulate cellular oxygen consumption rate and metabolism and provide a critical role in hypoxia signaling and tumor progression. J. Clin. Invest 122, 600–611. [PubMed: 22214851]
29. Sun Y, Li T, Xie C, Xu Y, Zhou K, Rodriguez J, Han W, Wang X, Kroemer G, Modjtahedi N, et al. (2017). Haploinsufficiency in the mitochondrial protein CHCHD4 reduces brain injury in a mouse model of neonatal hypoxia-ischemia. Cell Death Dis. 8, e2781. [PubMed: 28492551]
30. Arany Z, Lebrasseur N, Morris C, Smith E, Yang W, Ma Y, Chin S, and Spiegelman BM (2007). The transcriptional coactivator PGC-1beta drives the formation of oxidative type IIX fibers in skeletal muscle. Cell Metab. 5, 35–46. [PubMed: 17189205]
31. Grondard C, Biondi O, Pariset C, Lopes P, Deforges S, Lécolle S, Gaspera BD, Gallien CL, Chanoine C, and Charbonnier F (2008). Exercise-induced modulation of calcineurin activity parallels the time course of myofibre transitions. J. Cell. Physiol 214, 126–135. [PubMed: 17559060]
32. Rudnicki MA, Braun T, Hinuma S, and Jaenisch R (1992). Inactivation of MyoD in mice leads to up-regulation of the myogenic HLH gene Myf-5 and results in apparently normal muscle development. Cell 71, 383–390. [PubMed: 1330322]

33. Duquet A, Polesskaya A, Cuvellier S, Ait-Si-Ali S, Héry P, Pritchard LL, Gerard M, and Harel-Bellan A (2006). Acetylation is important for MyoD function in adult mice. EMBO Rep. 7, 1140–1146. [PubMed: 17028574]
34. Hughes SM, Koishi K, Rudnicki M, and Maggs AM (1997). MyoD protein is differentially accumulated in fast and slow skeletal muscle fibres and required for normal fibre type balance in rodents. Mech. Dev 61, 151–163. [PubMed: 9076685]
35. Ekmark M, Rana ZA, Stewart G, Hardie DG, and Gundersen K (2007). De-phosphorylation of MyoD is linking nerve-evoked activity to fast myosin heavy chain expression in rodent adult skeletal muscle. J. Physiol 584, 637–650. [PubMed: 17761773]
36. Gabriel K, Milenkovic D, Chacinska A, Müller J, Guiard B, Pfanner N, and Meisinger C (2007). Novel mitochondrial intermembrane space proteins as substrates of the MIA import pathway. J. Mol. Biol 365, 612–620. [PubMed: 17095012]
37. Modjtahedi N, Tokatlidis K, Dessen P, and Kroemer G (2016). Mitochondrial Proteins Containing Coiled-Coil-Helix-Coiled-Coil-Helix (CHCH) Domains in Health and Disease. Trends Biochem. Sci 41, 245–260. [PubMed: 26782138]
38. Modjtahedi N, Hangen E, Gonin P, and Kroemer G (2015). Metabolic epistasis among apoptosis-inducing factor and the mitochondrial import factor CHCHD4. Cell Cycle 14, 2743–2747. [PubMed: 26178476]
39. Guttridge DC, Mayo MW, Madrid LV, Wang CY, and Baldwin AS Jr. (2000). NF-kappaB-induced loss of MyoD messenger RNA: possible role in muscle decay and cachexia. Science 289, 2363–2366. [PubMed: 11009425]
40. Dogra C, Changotra H, Mohan S, and Kumar A (2006). Tumor necrosis factor-like weak inducer of apoptosis inhibits skeletal myogenesis through sustained activation of nuclear factor-kappaB and degradation of MyoD protein. J. Biol. Chem 281, 10327–10336. [PubMed: 16461349]
41. Sabir JSM, El Omri A, Shaik NA, Banaganapalli B, Al-Shaeri MA, Alkenani NA, Hajrah NH, Awan ZA, Zrelli H, Elango R, and Khan M (2019). Identification of key regulatory genes connected to NF-kappaB family of proteins in visceral adipose tissues using gene expression and weighted protein interaction network. PLoS One 14, e0214337. [PubMed: 31013288]
42. Potting C, Tatsuta T, König T, Haag M, Wai T, Aaltonen MJ, and Langer T (2013). TRIAP1/PRELI complexes prevent apoptosis by mediating intramitochondrial transport of phosphatidic acid. Cell Metab. 18, 287–295. [PubMed: 23931759]
43. Chen L, Dong J, Liao S, Wang S, Wu Z, Zuo M, Liu B, Yan C, Chen Y, He H, et al. (2022). Loss of Sam50 in hepatocytes induces cardiolipin-dependent mitochondrial membrane remodeling to trigger mtDNA release and liver injury. Hepatology 76, 1389–1408. [PubMed: 35313046]
44. Ohlsson L, Hall A, Lindahl H, Danielsson R, Gustafsson A, Lavant E, and Ljunggren L (2020). Increased level of circulating cell-free mitochondrial DNA due to a single bout of strenuous physical exercise. Eur. J. Appl. Physiol 120, 897–905. [PubMed: 32088743]
45. Zanini G, De Gaetano A, Selleri V, Savino G, Cossarizza A, Pinti M, Mattioli AV, and Nasi M (2021). Mitochondrial DNA and Exercise: Implications for Health and Injuries in Sports. Cells 10, 2575. [PubMed: 34685555]
46. Ge Z, Zhang Z, and Ding S (2022). Effect of acute endurance exercise and exhaustive exercise on innate immune signals induced by mtDNA. Eur. J. Inflammation 20, 1–11.
47. Hong Z, Mei J, Li C, Bai G, Maimaiti M, Hu H, Yu W, Sun L, Zhang L, Cheng D, et al. (2021). STING inhibitors target the cyclic dinucleotide binding pocket. Proc. Natl. Acad. Sci. USA 118, e2105465118. [PubMed: 34099558]
48. Keinan N, Tyomkin D, and Shoshan-Barmatz V (2010). Oligomerization of the mitochondrial protein voltage-dependent anion channel is coupled to the induction of apoptosis. Mol. Cell Biol 30, 5698–5709. [PubMed: 20937774]
49. Kim J, Gupta R, Blanco LP, Yang S, Shteinfer-Kuzmine A, Wang K, Zhu J, Yoon HE, Wang X, Kerkhofs M, et al. (2019). VDAC oligomers form mitochondrial pores to release mtDNA fragments and promote lupus-like disease. Science 366, 1531–1536. [PubMed: 31857488]
50. Ben-Hail D, Begas-Shvartz R, Shalev M, Shteinfer-Kuzmine A, Gruzman A, Reina S, De Pinto V, and Shoshan-Barmatz V (2016). Novel Compounds Targeting the Mitochondrial Protein VDAC1

Inhibit Apoptosis and Protect against Mitochondrial Dysfunction. J. Biol. Chem 291, 24986–25003. [PubMed: 27738100]

51. King MP, and Attardi G (1989). Human cells lacking mtDNA: repopulation with exogenous mitochondria by complementation. Science 246, 500–503. [PubMed: 2814477]
52. Betaneli V, Petrov EP, and Schwille P (2012). The role of lipids in VDAC oligomerization. Biophys. J 102, 523–531. [PubMed: 22325275]
53. Evans M, Cogan KE, and Egan B (2017). Metabolism of ketone bodies during exercise and training: physiological basis for exogenous supplementation. J. Physiol 595, 2857–2871. [PubMed: 27861911]
54. Sato Y, Ohtsubo H, Nihei N, Kaneko T, Sato Y, Adachi SI, Kondo S, Nakamura M, Mizunoya W, Iida H, et al. (2018). Apobec2 deficiency causes mitochondrial defects and mitophagy in skeletal muscle. FASEB J. 32, 1428–1439. [PubMed: 29127187]
55. Sun N, Yun J, Liu J, Malide D, Liu C, Rovira II, Holmström KM, Fergusson MM, Yoo YH, Combs CA, and Finkel T (2015). Measuring In Vivo Mitophagy. Mol. Cell 60, 685–696. [PubMed: 26549682]
56. He C, Bassik MC, Moresi V, Sun K, Wei Y, Zou Z, An Z, Loh J, Fisher J, Sun Q, et al. (2012). Exercise-induced BCL2-regulated autophagy is required for muscle glucose homeostasis. Nature 481, 511–515. [PubMed: 22258505]
57. Lira VA, Okutsu M, Zhang M, Greene NP, Laker RC, Breen DS, Hoehn KL, and Yan Z (2013). Autophagy is required for exercise training-induced skeletal muscle adaptation and improvement of physical performance. FASEB J. 27, 4184–193. [PubMed: 23825228]
58. Wang PY, Ma J, Kim YC, Son AY, Syed AM, Liu C, Mori MP, Huffstutler RD, Stolinski JL, Talagala SL, et al. (2023). WASF3 disrupts mitochondrial respiration and may mediate exercise intolerance in myalgic encephalomyelitis/chronic fatigue syndrome. Proc. Natl. Acad. Sci. USA 120, e2302738120. [PubMed: 37579159]
59. Shang R, Wang J, Sun W, Dai B, Ruan B, Zhang Z, Yang X, Gao Y, Qu S, Lv X, et al. (2016). RRAD inhibits aerobic glycolysis, invasion, and migration and is associated with poor prognosis in hepatocellular carcinoma. Tumour Biol. 37, 5097–5105. [PubMed: 26546438]
60. Feng X, Wei Z, Tao X, Du Y, Wu J, Yu Y, Yu H, and Zhao H (2021). PLAC8 promotes the autophagic activity and improves the growth priority of human trophoblast cells. FASEB J. 35, e21351. [PubMed: 33570788]
61. Abreu-Vieira G, Fischer AW, Mattsson C, de Jong JMA, Shabalina IG, Rydén M, Laurencikiene J, Arner P, Cannon B, Nedergaard J, and Petrovic N (2015). Cidea improves the metabolic profile through expansion of adipose tissue. Nat. Commun 6, 7433. [PubMed: 26118629]
62. Ehlers ML, Celona B, and Black BL (2014). NFATc1 controls skeletal muscle fiber type and is a negative regulator of MyoD activity. Cell Rep. 8, 1639–1648. [PubMed: 25242327]
63. Shintaku J, Peterson JM, Talbert EE, Gu JM, Ladner KJ, Williams DR, Mousavi K, Wang R, Sartorelli V, and Guttridge DC (2016). MyoD Regulates Skeletal Muscle Oxidative Metabolism Cooperatively with Alternative NF-kappaB. Cell Rep. 17, 514–526. [PubMed: 27705798]
64. West AP, and Shadel GS (2017). Mitochondrial DNA in innate immune responses and inflammatory pathology. Nat. Rev. Immunol 17, 363–375. [PubMed: 28393922]
65. Zhuang J, Wang PY, Huang X, Chen X, Kang JG, and Hwang PM (2013). Mitochondrial disulfide relay mediates translocation of p53 and partitions its subcellular activity. Proc. Natl. Acad. Sci. USA 110, 17356–17361. [PubMed: 24101517]
66. Cai D, Frantz JD, Tawa NE Jr., Melendez PA, Oh BC, Lidov HGW, Hasselgren PO, Frontera WR, Lee J, Glass DJ, and Shoelson SE (2004). IKKbeta/NF-kappaB activation causes severe muscle wasting in mice. Cell 119, 285–298. [PubMed: 15479644]
67. Park JY, Wang PY, Matsumoto T, Sung HJ, Ma W, Choi JW, Anderson SA, Leary SC, Balaban RS, Kang JG, and Hwang PM (2009). p53 improves aerobic exercise capacity and augments skeletal muscle mitochondrial DNA content. Circ. Res 105, 705–712. 11 p following 712, 711 p following 712. [PubMed: 19696408]
68. Frezza C, Cipolat S, and Scorrano L (2007). Organelle isolation: functional mitochondria from mouse liver, muscle and cultured fibroblasts. Nat. Protoc 2, 287–295. [PubMed: 17406588]

69. Dimauro I, Pearson T, Caporossi D, and Jackson MJ (2012).A simple protocol for the subcellular fractionation of skeletal muscle cells and tissue. BMC Res. Notes 5, 513. [PubMed: 22994964]

70. Patino WD, Mian OY, Kang JG, Matoba S, Bartlett LD, Holbrook B, Trout HH 3rd, Kozloff L, and Hwang PM (2005). Circulating transcriptome reveals markers of atherosclerosis. Proc. Natl. Acad. Sci. USA 102, 3423–3428. [PubMed: 15728378]

71. Maekawa H, Inoue T, Ouchi H, Jao TM, Inoue R, Nishi H, Fujii R, Ishidate F, Tanaka T, Tanaka Y, et al. (2019). Mitochondrial Damage Causes Inflammation via cGAS-STING Signaling in Acute Kidney Injury. Cell Rep. 29, 1261–1273.e6. [PubMed: 31665638]

72. Sun N, Malide D, Liu J, Rovira II, Combs CA, and Finkel T (2017). A fluorescence-based imaging method to measure in vitro and in vivo mitophagy using mt-Keima. Nat. Protoc 12, 1576–1587. [PubMed: 28703790]

73. Xia J, Sinelnikov IV, Han B, and Wishart DS (2015). MetaboAnalyst 3.0-making metabolomics more meaningful. Nucleic Acids Res. 43, W251–W257. [PubMed: 25897128]

Highlights

- CHCHD4 regulation by exercise training is necessary for oxidative fiber type switching
- Decreased import of TRIAP1 by CHCHD4 reduces cardiolipin and promotes VDAC oligomerization
- mtDNA release activates innate immune signaling to reduce MyoD for fiber type switching
- Haploinsufficiency of CHCHD4 in mice promotes oxidative muscle fibers and prevents obesity

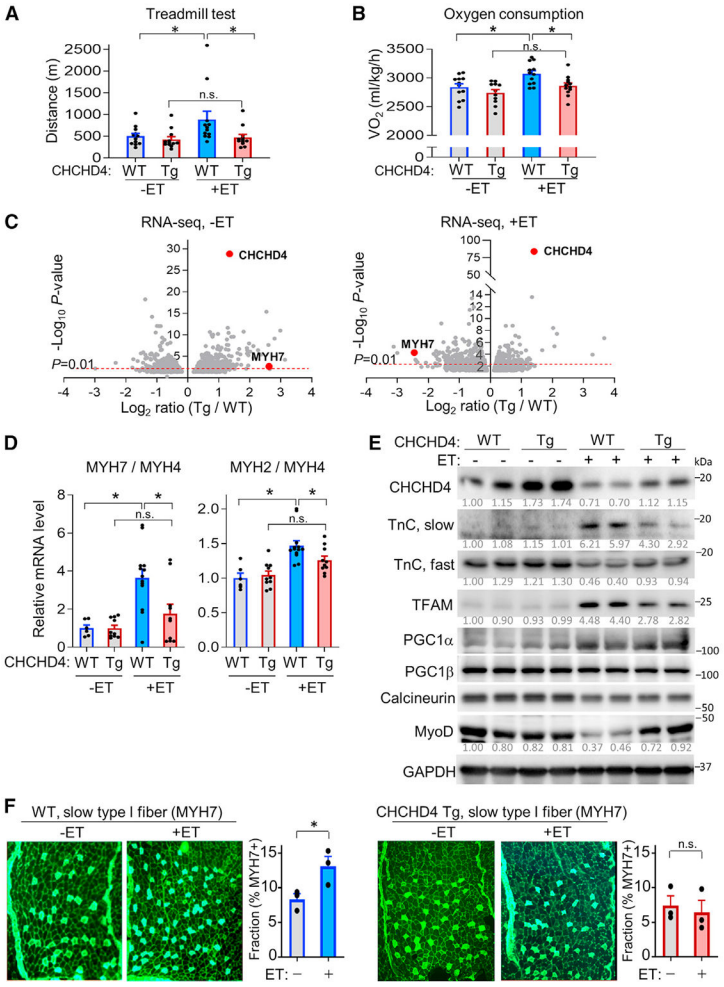

Figure 1. CHCHD4 overexpression prevents oxidative type fiber formation and MyoD reduction induced by exercise training in skeletal muscle

(A) Maximal treadmill running capacity was tested in WT and CHCHD4 Tg mice, without (−ET) or with (+ET) 4 weeks of treadmill exercise training (n = 12).

(B) Oxygen consumption rates (VO_2) of WT and Tg mice before (−ET) and after (+ET) 4 weeks of exercise training were measured in a metabolic chamber (CLAMS) during periods of increased activity (night cycle) (n = 11–12).

(C) Volcano plots of tibialis anterior muscle RNA-seq data (Tg/WT differentially expressed genes) without (−ET, left) or with (+ET, right) 4 weeks of exercise training (n = 4). Red dashed line indicates p = 0.01.

(D) Quantification of mRNA levels of type I fiber MYH7, type IIa fiber MYH2, and type IIb fiber MYH4 in triceps surae muscle (comprising gastrocnemius, plantaris, and soleus) of mice without (−ET) or with (+ET) 4 weeks of exercise training by real-time RT-PCR. The ratio of oxidative fiber MYH7 or MYH2 to glycolytic fiber MYH4 is shown (n = 6–13).

(E) Triceps surae muscle from the indicated mice without (−) or with (+) 4 weeks of exercise training were processed for immunoblotting. Muscle samples were harvested ~7–10 days after exercise training. Values under the corresponding protein bands indicate their relative levels. One experiment out of 2 is shown.

(F) Immunofluorescence of slow type I fibers (MYH7) in triceps surae muscle cross-sections of the indicated mice without (−ET) or with (+ET) 4 weeks of exercise training. Shown are representative images of the lateral head of the gastrocnemius muscle and quantification of the $MYH7^+$ fibers (n = 3).

Age-matched male mice (16–20 weeks old) were used for the experiments. Statistical difference by 2-way ANOVA (A, B, and D) or by 2-tailed Student's t test (F). Values are mean ± SEM. Nonsignificant (n.s.), *$p < 0.05$.

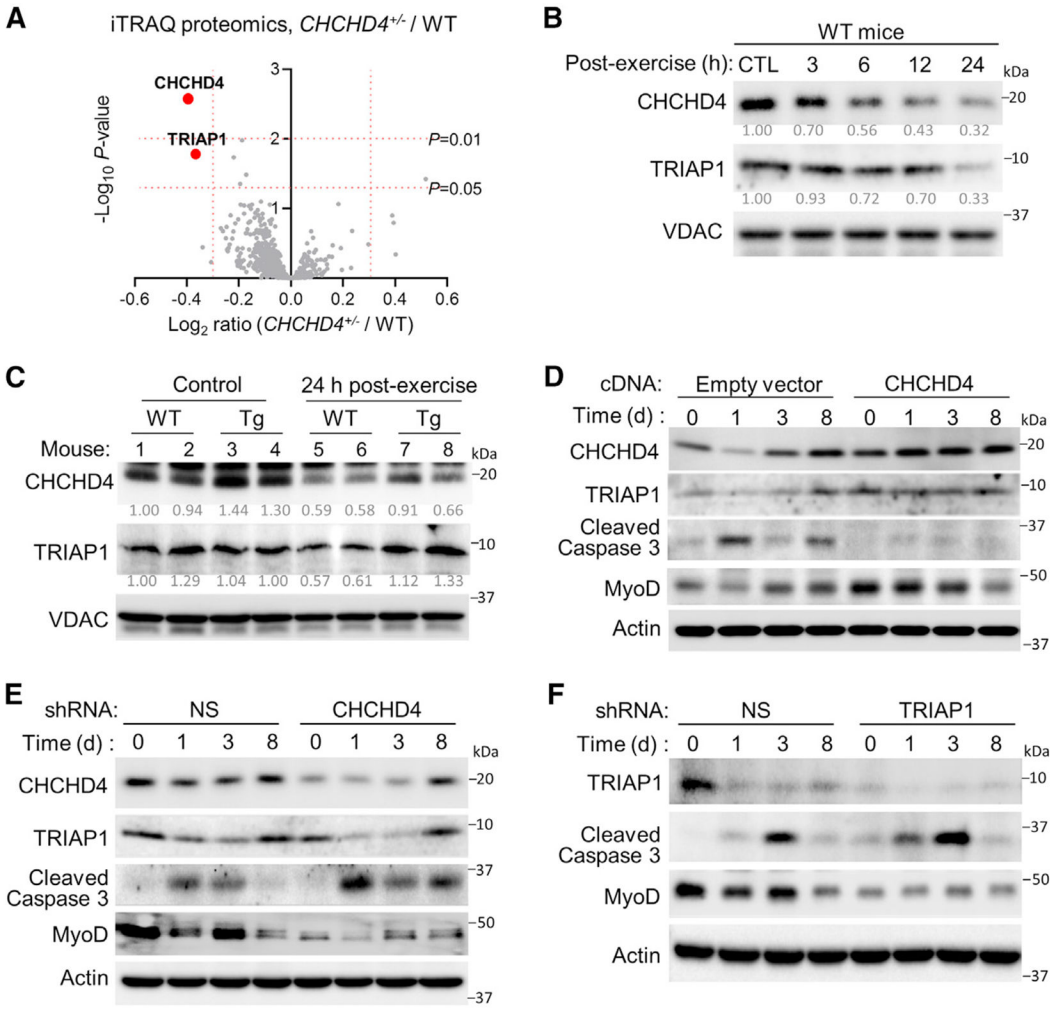

Figure 2. TRIAP1 mediates CHCHD4 regulation of MyoD level

(A) Volcano plots of iTRAQ proteomics data obtained from heart mitochondria of WT or *CHCHD4*$^{+/-}$ mice (~20-week-old males) treated with isoproterenol (n = 4). Red horizontal dashed lines show indicated p-values, and red vertical dashed lines show $\log_2$ ratio threshold of 0.3 (1.23 fold change).

(B) Male WT mice (~10 weeks old) were exercised for 1 h on a treadmill and then euthanized at the indicated times. Mitochondria purified from skeletal muscle were immunoblotted. Values under the corresponding protein bands indicate their relative levels. Unexercised control mice (CTL).

(C) Male WT and CHCHD4 Tg mice (~10 weeks old) were exercised for 1 h on a treadmill and then euthanized after 24 h together with unexercised control mice. Mitochondria were isolated from skeletal muscle and immunoblotted. Values under the corresponding protein bands indicate their relative levels.

(D–F) C2C12 cells were stably transduced with lentivirus containing the indicated cDNA or shRNA and cultured in 2% horse serum for the indicated time periods before immunoblotting.

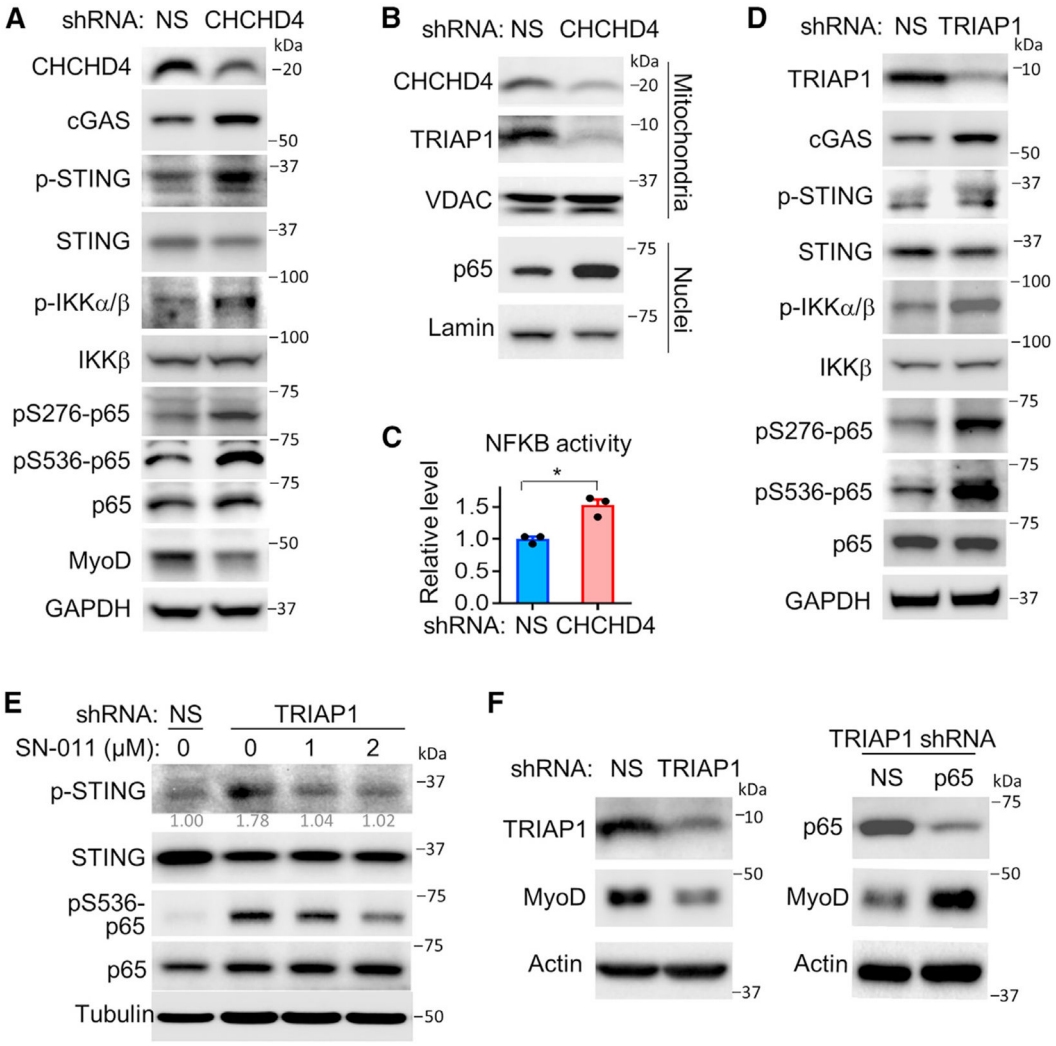

Figure 3. CHCHD4 and TRIAP1 regulate MyoD levels by activating cGAS-STING-NFKB pathway

(A) Immunoblot of C2C12 cells transduced with lentivirus expressing nonspecific (NS) or CHCHD4 shRNA.

(B) Immunoblot of mitochondria and nuclei isolated from C2C12 cells transduced with nonspecific (NS) or CHCHD4 shRNA lentivirus.

(C) DNA-binding activity of NFKB measured in the indicated cells (n = 3).

(D) Immunoblot of C2C12 cells transduced with NS or TRIAP1 shRNA lentivirus.

(E) Immunoblot of TRIAP1-depleted cells treated with STING antagonist SN-011 for 24 h. Values under the corresponding protein bands indicate their relative levels.

(F) Immunoblot of TRIAP1-depleted cells further transduced with NS or p65 shRNA lentivirus (right) compared with TRIAP1 shRNA alone (left) as control.

Graphs are representative of at least 3 experiments. Statistical difference by 2-tailed Student's t test. Values are mean ± SEM. *p < 0.01.

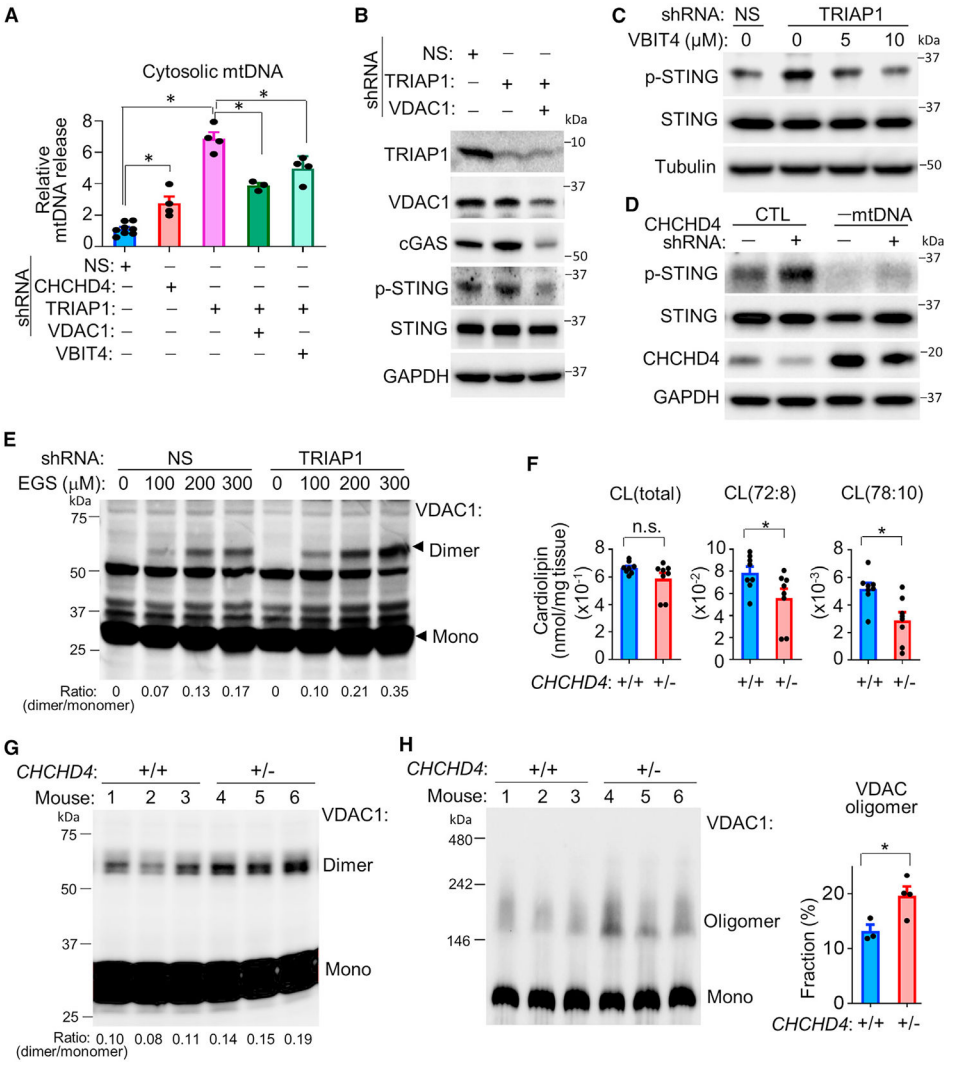

Figure 4. CHCHD4 and TRIAP1 activate the cGAS-STING pathway by promoting VDAC1 oligomerization and mtDNA release

(A) Relative mtDNA levels in the cytosol of C2C12 cells transduced with NS, CHCHD4, TRIAP1, or VDAC1 shRNA lentivirus, and the effect of treatment with 5 μM VBIT4, a VDAC oligomerization inhibitor, for 24 h (n = 4–8).

(B) Immunoblot of C2C12 cells transduced with NS, TRIAP1, or VDAC1 shRNA lentivirus.

(C) Immunoblot of TRIAP1-depleted cells treated with the indicated concentration of VBIT4 for 24 h.

(D) Immunoblot of control (CTL) and mtDNA-depleted (-mtDNA) C2C12 cells transduced with NS (−) or CHCHD4 shRNA lentivirus.

(E) C2C12 cells transduced with NS or TRIAP1 shRNA lentivirus were treated with the protein crosslinker EGS and resolved by SDS-PAGE for VDAC1 immunoblotting. (See Figure S8 for lower exposure image.).

(F) CLs in triceps surae muscle of WT and *CHCHD4*$^{+/-}$ mice (~20-week-old males) were measured using mass spectrometry (n = 8).

(G) Mitochondria isolated from triceps surae muscle of WT and *CHCHD4*$^{+/-}$ mice (~20-week-old males) were treated with 150 μM EGS and then resolved by SDS-PAGE for VDAC1 immunoblotting (n = 3). (See Figure S8 for lower exposure image.).
(H) Mitochondria from triceps surae muscle of WT and *CHCHD4*$^{+/-}$ mice (~20-week-old males) were solubilized in digitonin and Triton X-100 and then subjected to native PAGE for VDAC1 immunoblotting. The relative fraction of oligomerized VDAC1 was quantified (n = 3–4).
Statistical difference by 1-way ANOVA (A) or two-tailed Student's t test (F and H). Values are mean ± SEM. *$p < 0.01$ for the indicated groups.

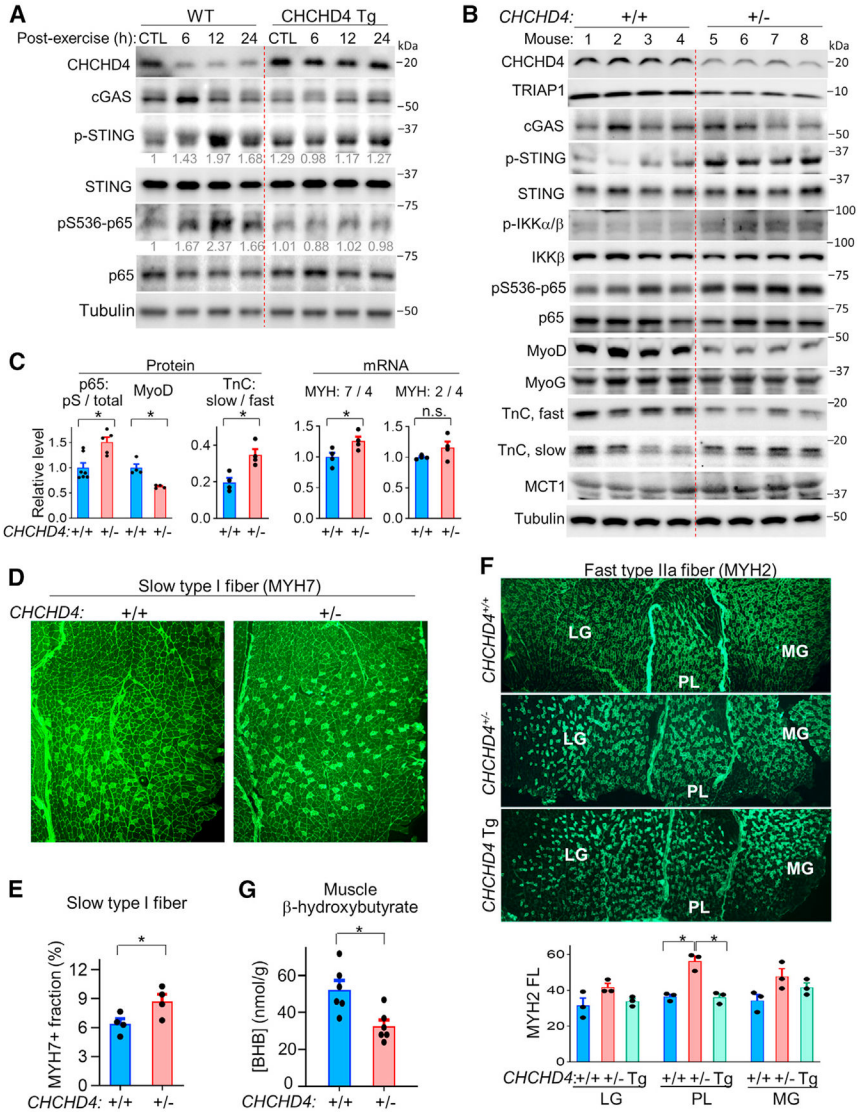

Figure 5. CHCHD4 haploinsufficiency mimics exercise by activating the cGAS-STING-NFKB pathway and increasing oxidative muscle fibers

(A) WT and CHCHD4 Tg mice (~20-week-old males) were exercised on a treadmill for 1 h. At the indicated times after exercise, the triceps surae muscles were isolated for immunoblotting. Values under the corresponding protein bands indicate their relative levels. One experiment out of 2 is shown.

(B) The triceps surae muscles of *CHCHD4*$^{+/+}$ and *CHCHD4*$^{+/-}$ mice (~20-week-old males) without exercise training were processed for immunoblotting (n = 4). One experiment out of 2 is shown.

(C) Phosphorylated p65 (pS), MyoD, and TnC (slow or fast isoform) proteins in the immunoblots (B) were quantified (n = 4–7). In addition, the mRNA levels of MYH7, MYH2, and MYH4 in the triceps surae muscle were quantified by real-time RT-PCR (n = 4). The relative ratios of these markers are shown.

(D) Representative MYH7 immunofluorescence cross-sectional images of the gastrocnemius medial head of the indicated mouse genotype (~20-week-old males).

(E) Quantification of the $MYH7^{+}$ fibers in (D) (n = 4).
(F) MYH2 immunofluorescence in triceps surae muscle cross-sections of the indicated mouse genotypes (~20-week-old males). Representative images of the lateral and medial head of the gastrocnemius (LG, MG) and the plantaris (PL) are shown. Lower graph shows quantification of the MYH2 fluorescence (FL) signal (n = 3).
(G) β-Hydroxybutyrate levels in the triceps surae muscle of *CHCHD4*$^{+/+}$ and *CHCHD4*$^{+/-}$ mice (~1 year old) were measured by time-of-flight mass spectrometry (n = 6).
Statistical difference by two-tailed Student's t test. Values are mean ± SEM. *$p < 0.05$.

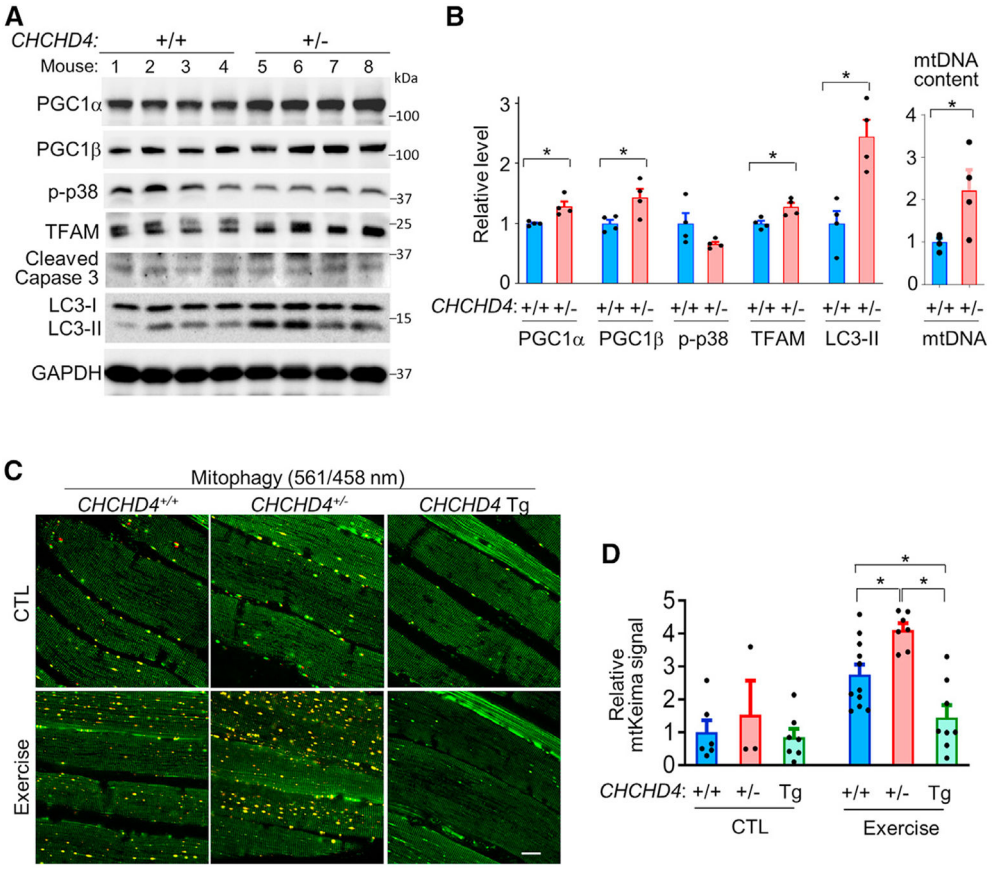

Figure 6. CHCHD4 haploinsufficiency promotes mitochondrial biogenesis

(A) Immunoblots of mitochondrial biogenesis factors in the triceps surae muscle of *CHCHD4*$^{+/+}$ and *CHCHD4*$^{+/-}$ mice.

(B) Quantification of relative protein levels shown in (A) and the corresponding mtDNA content.

(C) Effect of CHCHD4 genotype on mitophagy *in vivo* imaged by mt-Keima fluorescence signal in skeletal muscle without (control, CTL) or with 60 min of treadmill exercise (measured 12 h after exercise). The red (acidic pH):green (neutral pH) fluorescence ratio (561/458 nm) indicates mitophagy activity.

(D) Quantification of red:green fluorescence ratio in (C) is shown ($n \geq 3$). Statistical comparisons by two-tailed Student's t test (B) or by 1-way ANOVA. Values are mean ± SEM. *$p < 0.05$. Scale bar, 40 μm.

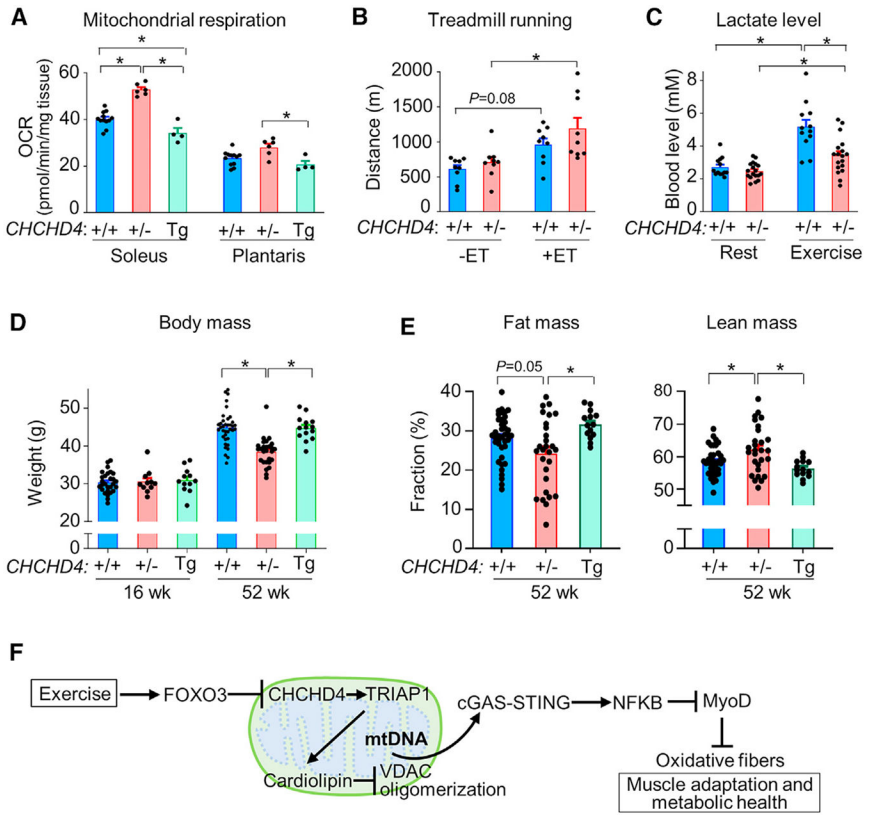

Figure 7. CHCHD4 haploinsufficiency confers beneficial effects of exercise

(A) *Ex vivo* basal OCRs of whole soleus and plantaris muscle of *CHCHD4*$^{+/+}$, *CHCHD4*$^{+/-}$, and CHCHD4 Tg mice (~20-week-old males) (n = 4–12).

(B) Maximal treadmill running capacity of *CHCHD4*$^{+/+}$ and *CHCHD4*$^{+/-}$ mice (~1 year old) before (−ET) and after (+ET) 8 weeks of voluntary wheel running (n = 9).

(C) Blood lactate levels of the indicated mice (~12 weeks old) before and after submaximal treadmill exercise (n = 11–12).

(D) Body weight of *CHCHD4*$^{+/+}$, *CHCHD4*$^{+/-}$, and CHCHD4 Tg mice at the indicated ages (n = 11–37).

(E) Body mass composition of *CHCHD4*$^{+/+}$, *CHCHD4*$^{+/-}$, and CHCHD4 Tg mice at age ~52 weeks (n = 14–39).

(F) Model of the mechanism by which CHCHD4 regulates skeletal muscle adaptation to exercise training for improving oxidative metabolism. Exercise training, previously shown to downregulate CHCHD4 via FOXO3 transcription factor, can decrease TRIAP1 levels, thereby inducing VDAC oligomerization and mtDNA release into cytosol, with activation of the innate immune pathway and NFKB. NFKB is known to downregulate MyoD, which results in higher levels of oxidative fibers in skeletal muscle for aerobic metabolism and could prevent obesity.

Male mice were used for all of the experiments. Statistical difference by 2-way ANOVA (A–D) or 1-way ANOVA (E). Values are mean ± SEM. *p < 0.05.

KEY RESOURCES TABLE

REAGENT or RESOURCE	SOURCE	IDENTIFIER
Antibodies		
Actin	Sigma-Aldrich	A1978; RRID:AB_476692
cGAS	Cell Signaling	31659; RRID:AB_2799008
Calcineurin A	Cell Signaling	2614; RRID:AB_22168458
CHCHD4	Novus	NBP1-83537; RRID:AB_11038981
Cleaved caspase-3	Cell Signaling	9664; RRID:AB_2070042
GAPDH	Ambion	AM4300; RRID:AB_2536381
IKKβ	Cell Signaling	8943; RRID:AB_11024092
Lamin B1	Abcam	ab16048; RRID:AB_443298
LC3	Sigma	L8918; RRID:AB_1079382
MCT1	Proteintech	20139-1-AP; RRID:AB_2878645
MYH2	DSHB	SC-71; RRID:AB_2147165
MYH4	DSHB	BF-F3; RRID:AB_2266724
MYH7	DSHB	BA-D5; RRID:AB_2235587
MyoD	Novus	NBP1-54153; RRID:AB_11015772
MyoG	Santa Cruz	sc-12732; RRID:AB_627980
p65	Thermo Fisher Scientific	33-9900; RRID:AB_2533153
PGC1α	Cell Signaling	2178; RRID:AB_823600
PGC1β	Abcam	ab176328; RRID:AB_2893194
p-p38	Cell signaling	9211; RRID:AB_331641
pS176/180-IKKα/β	Cell Signaling	2697; RRID:AB_2079382
pS276-p65	Invitrogen	PA5-37718; RRID:AB_2554326
pS365-STING	Cell Signaling	72971; RRID:AB_2799831
pS536-p65	Cell Signaling	3036; RRID:AB_331281
STING	Cell Signaling	50494; RRID:AB_2799375
TFAM	Abcam	ab131607; RRID:AB_11154693
TRIAP1	Proteintech	15351-1-AP; RRID:AB_2878129
Troponin C fast	Santa Cruz	sc-48347; RRID:AB_628400
Troponin C slow	Santa Cruz	sc-52265; RRID:AB_2206089
Tubulin	Sigma-Aldrich	T5168; RRID:AB_477579
VDAC	Rockland	600-401-882; RRID:AB_2304361
VDAC1	Abcam	ab14734; RRID:AB_443084
Chemicals, peptides, and recombinant proteins		
Fetal bovine serum	Thermo Fisher Scientific	16000044
Horse serum	Thermo Fisher Scientific	16050122
Dulbecco's Modified Eagle Medium	Thermo Fisher Scientific	10569044
Puromycin	Thermo Fisher Scientific	A1113803
Hygromycin	Thermo Fisher Scientific	10687010
Fugene HD transfection	Promega Corporation	E2311
ECL Plus Western Blotting	Pierce	M0053-10

REAGENT or RESOURCE	SOURCE	IDENTIFIER
VBIT-4	AOBIOUS	AOB820
STING antagonist SN-001	Cayman, Inc	34890
Digitonin	Tokyo Chemical Industry	300410
EGS Crosslinker	ProteoChem	c1130
Critical commercial assays		
RNeasy kit	Qiagen	74104
DNeasy Blood & Tissue Kit	Qiagen	69504
SuperScript Double-Stranded cDNA Synthesis Kit	Thermo Fisher Scientific	11917010
QuikChange II Site-Directed Mutagenesis Kit	Agilent	200523
In-Fusion HD Cloning Plus	Takara	638920
NFKB Transcription Factor Assay kit	Cayman	10007889
beta Hydroxybutyrate A Assay Kit (Colorimetric)	Abcam	ab83390
Mouse Cytokine Array Kit	R&D Systems	ARY006
Deposited data		
Cardiolipin Analysis	This paper	https://doi.org/10.25444/nhlbi.24402901
Metabolome Analysis	This paper	https://doi.org/10.25444/nhlbi.24402901
ITRAQ_WT vs. CHCHD4Tg	This paper	https://doi.org/10.25444/nhlbi.24402901
ITRAQ_WT vs. *CHCHD4*$^{+/-}$	This paper	https://doi.org/10.25444/nhlbi.24402901
RNA-seq of WT vs. CHCHD4 Tg	This paper	GEO: GSE245760
Experimental models: Cell lines		
C2C12	ATCC	CRL-1772
293T	ATCC	CRL-3216
Experimental models: Organisms/strains		
Mouse: *CHCHD4*$^{+/-}$	Texas Institute for Genomic Medicine	IST11943B12
Mouse: C57BL6/J	Jackson Laboratory	JAX 000664
Mouse: mt-Keima transgenic (strain FVB/NJ)	Sun et al.[55]	Toren Finkel, University of Pittsburgh
Mouse: CHCHD4 transgenic (strain C57BL6/J)	Zhuang et al.[26]	N/A
Oligonucleotides		
See Table S9	This paper	N/A
Recombinant DNA		
Mouse p53 shRNA lentiviral plasmid	OpenBiosystems	TRCN0000012361
Lentiviral Packaging Mix	Sigma-Aldrich	SHP001
pBROAD3	InvivoGen	pbroad3
CHCHD4 shRNA & control vector	Horizon Discovery	RMM4431-200361800 & RHS4348
CHCHD4 cDNA & control vector	GeneCopoeia	EX-Mm10785-Lv105 & EXNEG- Lv105
TRIAP1 shRNA & control vector	GeneCopoeia	MSH034752-LVRH1H & CSHCTR001-LVRH1H
VDAC1 shRNA & control vector	GeneCopoeia	MSH096502-LVRU6P & CSHCTR001-LVRU6P
Software and algorithms		
GraphPad Prism 7.0	GraphPad Software	N/A
MetaboAnalyst 3.0	MetaboAnalyst	N/A

REAGENT or RESOURCE	SOURCE	IDENTIFIER
STAR/2.7.8a	RNA sequence alignment	N/A
RSEM/1.3.2	Quantifying gene and isoform expression levels	N/A
DAVID Bioinformatics Resources	National Institutes of Health	N/A
R	https://www.r-project.org/	N/A
ImageJ	ImageJ software	N/A
Thermo Proteome Discoverer 2.4	proteomics research	N/A
Others		
Rodent Diet with 60 kcal% Fat	Research Diets	D12492
Comprehensive Laboratory Animal Monitoring System (CLAMS)	Columbus Instruments	N/A
Treadmill exercise Exer-3/6	Columbus Instruments	1050-SU-D65
Minispec NMR analyzer	Bruker	N/A
Lactate Pro Analyzer	Arkray	SKU: LacPro